

Implications for the collisional strength of Jupiter Trojans from the Eurybates family

Raphael Marschall^{1,2}, David Nesvorný¹, Rogerio Deienno¹, Ian Wong³, Harold F. Levison¹, and William F. Bottke¹

¹Southwest Research Institute, 1050 Walnut St, Suite 300, Boulder, CO 80302, USA

²CNRS, Observatoire de la Côte d’Azur, Laboratoire J.-L. Lagrange, CS 34229, 06304 Nice Cedex 4, France; raphael.marschall@oca.eu

³Department of Earth, Atmospheric, and Planetary Sciences, Massachusetts Institute of Technology, Cambridge, MA 02139, USA

August 16, 2022

Abstract

In this work, we model the collisional evolution of the Jupiter Trojans and determined under which conditions the Eurybates-Queta system survives. We show that the collisional strength of the Jupiter Trojans and the age of the Eurybates family and by extension Queta are correlated.

The collisional grinding of the Jupiter Trojan population over 4.5 Gy results in a size-frequency distribution (SFD) that remains largely unaltered at large sizes (> 10 km) but is depleted at small sizes (10 m to 1 km). This results in a turnover in the SFD, the location of which depends on the collisional strength of the material. It is to be expected that the Trojan SFD bends between 1 and 10 km.

Based on the SFD of the Eurybates family, we find that the family was likely the result of a catastrophic impact onto a 100 km rubble pile target. This corresponds to objects with a rather low collisional strength (10 times weaker than that of basaltic material studied in [Benz & Asphaug, 1999](#)).

Assuming this weak strength, and an initial cumulative slope of the size frequency distribution of 2.1 between diameters of 2 m and 100 km when the Trojans were captured, the existence of Queta, the satellite of Eurybates, implies an upper limit for the family age of 3.7 Gy.

Alternatively, we demonstrate that an unconventional collisional strength with a minimum at 20 m is a plausible candidate to ensure the survival of Queta over the age of the Solar System.

Finally, we show how different collisional histories change the expected number of craters on the targets of the Lucy mission and that Lucy will be able to differentiate between them.

1 Introduction

The Lucy mission ([Levison et al., 2017](#)) will be the first mission to study Jupiter Trojans (JT) up close. During five encounters for seven Jupiter Trojans between 2027 and 2033 it will sample the diversity of Trojans. The targets include (3548) Eurybates a C-type Trojan and the largest member of a collisional family ([Brož & Rozehnal, 2011](#)), (11351) Leucus, and (21900) Orus, two D-type Trojans, (15094) Polymele, a P-type Trojan, and (617) Patroclus and Menoetius, an almost equal mass binary pair that is also a P-type. Polymele is the smallest target ($D \sim 21$ km), whereas Patroclus is the largest ($D \sim 140$ km). Leucus stands out for its very long rotation period (~ 445 h; [Buie et al., 2018](#); [Mottola et al., 2020](#)). Lucy has several objectives with the Trojans: (i) It will map the colors, albedos, and shapes of the target bodies; (ii) It will determine the distribution of minerals, ices and organics on

each target surface; (iii) It will measure the crater size frequency distributions (SFD) on each target body to determine the relative ages of different parts of their surfaces, and (iv) it will measure the masses and bulk densities of its targets as well as search for satellites and rings around them.

Jupiter Trojans are outer solar system planetesimals that orbit the Sun in a 1:1 resonance with Jupiter. They are found in two swarms around the L_4 and L_5 Lagrangian points of the Sun-Jupiter system where they lead/trail Jupiter by 60° respectively (Lagrange, 1772). Jupiter Trojans are known to be quite stable over the age of the solar system with only $\sim 25\%$ having escaped the resonance since they were captured (Levison et al., 1997; Di Sisto et al., 2014; Holt et al., 2020). Currently we know of roughly 9,400 Jupiter Trojans ($\sim 3,000$ larger than 10 km; Emery et al., 2015) making the population smaller than e.g. the main belt asteroid population ($\sim 10,000$ larger than 10 km; Bottke et al., 2015). Further, the L_4 swarm, with $\sim 1,800$ Trojans larger than 10 km, appears to have more objects than the L_5 swarm, with $\sim 1,200$ larger than 10 km (Jewitt et al., 2000; Yoshida & Nakamura, 2008; Yoshida & Terai, 2017).

The JTs show a bi-modal color distribution (“red” and “less red” Szabó et al., 2007; Roig et al., 2008; Emery et al., 2011; Wong et al., 2014; Jewitt, 2018). While the “red” Trojans overlap with “red” Kuiper belt objects (KBOs) and Centaurs, the “less-red” Trojan population does not have a clear analogue in the KBO population (Fig. 1 in Wong & Brown, 2016). There is no analogue for the “very red” KBOs in the JTs.

The Eurybates family is a cluster of C-type fragments with similar orbits within the L_4 swarm. Their members not only have inclinations that are tightly confined to $7.5^\circ \pm 0.5^\circ$, but they are also bluer than the “less-red” JTs. This makes them fairly exceptional within the Trojans.

Jupiter Trojans overall have very dark surfaces with visible albedos of 0.07 ± 0.03 , according to data from the WISE infrared survey spacecraft (Grav et al., 2011). The large JTs are darker with albedos around 0.05 while small JTs are on average “brighter” with albedos around 0.1 but with a wide scatter between 0.03 and 0.2 (Fig. 7 in Grav et al., 2011). JTs also have similar albedos and colors to comets (Fornasier et al., 2007, 2015). JTs populate the full stable region of around the Lagrange points, including high inclinations (30°), but typically have low eccentricities (< 0.15). The strong excitation in inclinations is an important constraint on the origin of Jupiter Trojans.

Dynamical models suggest Jupiter Trojans are unlikely to have formed at their current location (Marzari et al., 2002). This has led several groups to propose different origin scenarios and capture mechanisms. For example, in the “jumping Jupiter” model (Gomes et al., 2005; Tsiganis et al., 2005; Morbidelli et al., 2005; Nesvorný et al., 2013) the primordial Kuiper belt beyond Neptune gets scattered by the giant planet instability. One part of the population is scattered outwards into the trans-Neptunian object (TNO) region which includes the Edgeworth-Kuiper belt. Another part is scattered inwards. It is there where Jupiter, that jumps in semi-major axis, can capture some of these objects in the 1:1 resonance. This scenario would also imply that KBOs and Jupiter Trojans have a common origin but later evolved differently resulting in different colors, e.g. due to the different collisional (Wong & Brown, 2016) and thermophysical environment. The advantage of this model lies in the fact that it accurately predicts both the population size of the Jupiter Trojans and their orbital distribution, in particular their large range of inclinations. In a second fairly recent model proposed by Pirani et al. (2019), Jupiter forms at ~ 20 au or farther and subsequently migrates to its current location while growing in mass and sweeping up planetesimals in the process and capturing them in the 1:1 resonance. This model accounts for the asymmetry in the size of the two Trojan swarms (see Fig. 1), but the captured bodies do not reproduce the observed masses or the inclinations of the observed Trojans.

In this work we study the collisional evolution of the Jupiter Trojans and the Eurybates family to understand their implications for i) their material strength, and ii) the age of the Eurybates family and newly discovered satellite Queta (Noll et al., 2020). Queta’s survival has implications for the family forming event. We find that to a degree the age and strength of the Eurybates family and Queta are correlated and moreover depend on the SFD of the Jupiter Trojans at small sizes (< 1 km).

2 Constraints from the Trojans, Eurybates family, and Queta

Three constraints are of particular importance for this work:

1. the SFD of the Jupiter Trojans;
2. the Eurybates family and its SFD; and
3. the existence of Queta, the satellite of Eurybates.

We will present these constraints in the order given above which also corresponds to going from a macro to the micro view.

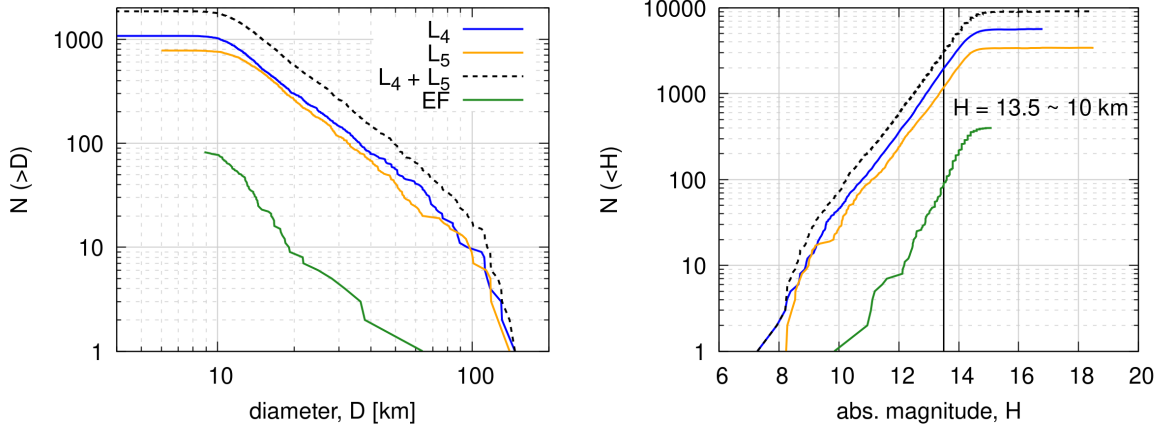


Figure 1: Left panel: The cumulative size-frequency distribution (SFD) as a function of diameter based on the WISE data (Grav et al., 2011) of the L_4 (blue line) and L_5 (orange line) Jupiter Trojan swarms are shown. The dashed black line shows the combined Trojan SFD and the green line the one of the Eurybates family (EF). The WISE data is complete down to about 20 km. Right panel: The cumulative SFD as a function of absolute magnitude, H , according to the data from the Minor Planet Center is shown. An absolute magnitude of 13.5 corresponds roughly to a 10 km Trojan, assuming an average albedo of 0.07 (Grav et al., 2011). The line colors correspond to the same (sub-) populations as in the left panel.

2.1 The Jupiter Trojan SFD

First, Figure 1 shows the cumulative SFD of the two Trojan swarms using the WISE data (Grav et al., 2011). We often find that SFDs follows a power law where the number of objects larger than a certain diameter can be written as

$$N(> D) = C_0 D^{-q}; \quad C_0 = N_0 D_0^q; \quad (1)$$

where q is the cumulative power law exponent or slope, and C_0 is the normalization constant such that for a reference diameter, D_0 , the number of objects larger than D_0 is N_0 . The differential power-law exponent, p , differs with respect to the cumulative power-law exponent by one: $p = q + 1$.

The Jupiter Trojan SFD has a well-defined cumulative slope of $q = 2.1$ between 10 – 100 km for both the L_4 and L_5 swarms (Fig. 1). At larger sizes the slope becomes steeper (similar to the KBO SFD) but is poorly defined because of the limited number of objects. Note that 100 km planetesimals are thought to be the preferred size (e.g. Morbidelli et al., 2009a; Klahr & Schreiber, 2020, 2021) for the formation of planetesimals by streaming instability (Youdin & Goodman, 2005). On the other end of the size range the population of small Trojans has been explored for L_4 (Jewitt et al., 2000; Yoshida & Nakamura, 2008; Wong & Brown, 2015; Yoshida & Terai, 2017). The latter three studies find that the slope of the SFD continues below 10 km, below which there is some indications that the SFD might become shallower. Unfortunately, the papers do not agree where (or if) this turnover takes place. The latest study (Yoshida & Terai, 2017), which uses the powerful Hyper Suprime-Cam attached to the Subaru Telescope, finds that a single power law is a better overall fit than a broken

power law. It remains uncertain whether a bend in the Jupiter Trojan SFD has actually been detected. If such a turnover exists it remains an open question how it relates to the observed turnover in the Edgeworth-Kuiper belt which occurs at roughly 1 km (Singer et al., 2019; Morbidelli et al., 2021).

2.2 The Eurybates family

Second, we discuss the Eurybates family. To identify the family we use the proper elements computed by Mira Brož (Holt et al., 2020) using the hierarchical clustering method (HCM, Zappala et al., 1990; Nesvorný et al., 2015) with a cutoff of 40 m/s. We have varied the cutoff to probe the change in family definition. Increasing the cutoff leads to clustering in the wider neighborhood while a smaller cutoff leaves out many peripheral members. In total the HCM identified 400 family members which roughly doubles the family members previously found by Nesvorný et al. (2015). This change reflects the increased number of known JTs since the time of that paper. The full list of family members with relevant properties presented in this work can be found in Tables 3 and 4.

The Eurybates family is well defined with respect to the proper elements (Fig. 2) and is roughly located in $a_{prop} \in [5.27 \text{ au}, 5.32 \text{ au}]$, $e_{prop} \in [0.032, 0.066]$, and $i_{prop} \in [6.99^\circ, 7.86^\circ]$.

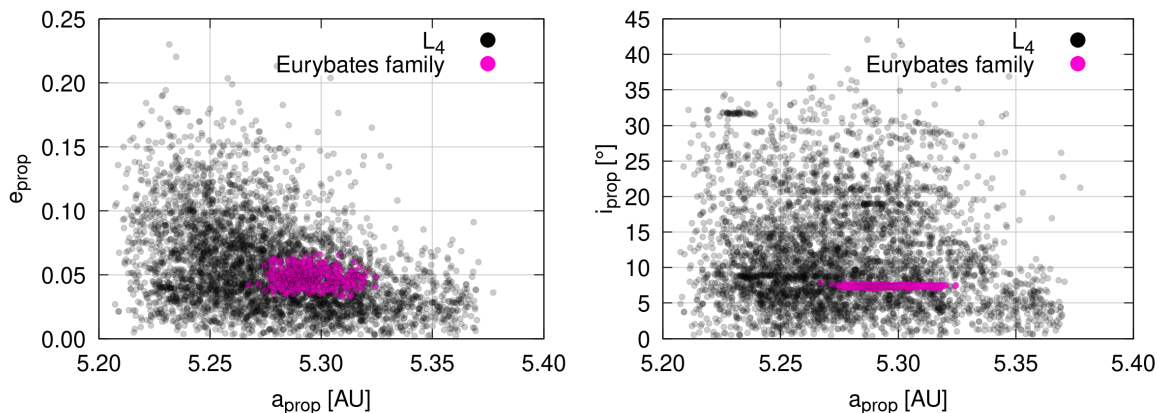


Figure 2: The proper elements of the L₄ swarm (black circles) and the Eurybates family (pink circles) are shown. The left panel shows the proper semi-major axis, a_{prop} , and proper eccentricity, e_{prop} , while the right panel shows the proper inclination, i_{prop} . The family is particularly well defined in inclination and hence easily stands out in the right panel.

The family is located close to the edge of the stable orbit region (Fig. 2, and Robutel & Gabern, 2006). In inclination the family is extremely well defined (within half a degree for most members; Brož & Rozehnal, 2011) and thus stands out in the right panel of Fig. 2.

Figure 3 shows the SFD of the Eurybates family as retrieved by the HCM (red line in left panel). This raw SFD has a shallow slope between 20 – 60 km of $q \sim 2.1$, similar to the overall JT slope (Fig. 1). At small sizes the SFD steepens up to a slope of $q \sim 3.7$, a value that is steeper than that of the L₄ Trojans. Slopes steeper than those of the background population are a common property of collisional families (Durda et al., 2007).

Before going any further, we need to establish if some of the identified members could be interlopers. This is particularly important for the largest family member because the shape of the SFD at those sizes can be diagnostic of the family forming collision itself (e.g. Benavidez et al., 2012).

To validate the possible detection of interlopers we first assess the likelihood of the background L₄ population contaminating the Eurybates family region. We have used the following dynamical constraint to determine the background population. First, we defined an ellipsoid in proper (a, e, i)-space to encircle the family. The center of the ellipsoid was placed at $(a, e, i) = (5.30 \text{ au}, 0.049, 7.4^\circ)$ and the respective radii set to $(R_a, R_e, R_i) = (0.069 \text{ au}, 0.040, 1.04^\circ)$. These values were chose to maximize the number of family members identified by HCM and minimizing the number of false deflections. All JTs within this ellipsoid were considered as a simplified definition of the family members and only slightly differed from the actual family members determined by HCM. We then increased the volume of the ellipsoid by a factor of eight by increasing the radii by a factor of two in each dimension. The

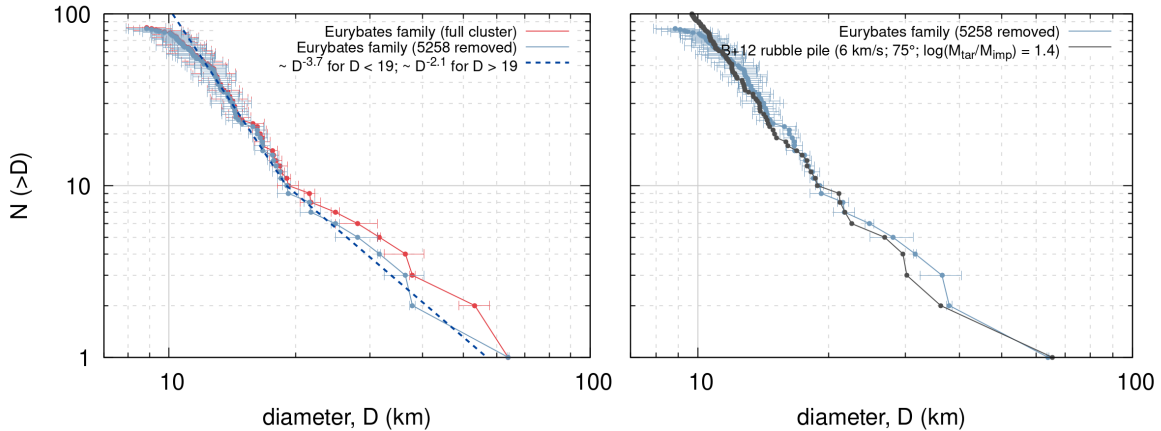


Figure 3: The left panel shows the SFDs of the Eurybates family with (i) all members retrieved by the HCM (red solid line and points) and (ii) suspected interloper (5258) Rhoeo removed from the family (blue solid line and points). The latter corresponds to our nominal case of the Eurybates family. The dashed line shows the approximate best power law fit for the nominal SFD with a slope of 2.1 for objects larger than 19 km and 3.7 below that. The right panel shows a comparison of our nominal SFD with the results from the rubble pile simulation of [Benavidez et al. \(2012\)](#) at an impact speed of 6 km/s, impact angle of 75° , and mass ratio of target to impactor bodies $\log(M_{tar}/M_{imp}) = 1.4$. The diameters and associated errors were taken from the NEOWISE data set v2.0 ([Mainzer et al., 2019](#)).

Trojan density within this larger volume minus the family volume was used to estimate the number of interlopers we can expect in the family. For objects with magnitude $H < 12$ we expect on average 1.4 interlopers. We also determined the probability of having N interlopers. There is a 40% chance that $N \geq 2$, and a 20% chance that $N \geq 3$. Consequently there is a non-negligible probability that there could be at least three large interlopers in the family. Over all sizes about 8% of the family members might be interlopers.

To investigate which of the largest members might be interlopers, we inspected their proper orbital elements as well as color data (Fig. 4).

We find that the second brightest/largest object identified by HCM, (5258) Rhoeo, is clearly displaced in proper inclination and eccentricity with respect to the center of the family. This would imply, that a very large fragment from the family forming event would have been ejected at a high speed. That is not to be expected. Collisional families typically have their largest members in center of the orbital element distribution (e.g. [Milani et al., 2017](#)). That is a consequence of the velocity distribution being a function of $1/D$. We hence strongly suspect that (5258) Rhoeo is an interloper. This conclusion is strengthened by its anomalous color compared to the other family members.

We collected colors from the Sloan Digital Sky Survey, SDSS ([Ivezić et al., 2001](#)), spectral slopes between 0.3 to 0.9 μm ([Fornasier et al., 2007](#)), and colors from the Zwicky Transient Facility Observations, ZTF ([Schemel & Brown, 2021](#)). The SDSS g-i color (top panel in Fig. 4) and the spectral slopes from [Fornasier et al. \(2007\)](#) (middle panel in Fig. 4) are connected and thus their color scales have been chosen such that they correspond to each other. The color scale of the ZTF data cannot be directly compared to the other two.

Eurybates and the bulk of the family have ZTF g-r of ~ 0.5 whereas (5258) Rhoeo has 0.6 which is significantly redder. This together with the orbital displacement of (5258) Rhoeo previously discussed provides strong evidence that it is indeed an interloper.

The Eurybates family is significantly bluer than the overall L_4 population (Fig. 5). With a g-i color of 0.96 ± 0.09 (313024) 2000 AV210 is on the very red end of the color distribution and thus another likely interloper. It has a diameter of 10.805 ± 0.599 and will thus not affect the family SFD and the work described here.

There are two other family members that might be interlopers. (8060) Anius has a somewhat larger eccentricity (middle panel in Fig. 4) but its ZTF color is close to the average color of the family. It is therefore unclear if (8060) Anius is indeed an interloper. We leave this as an open question. Future survey data might be able to provide additional insights. Similarly, (9818) Eurymachos has a slightly

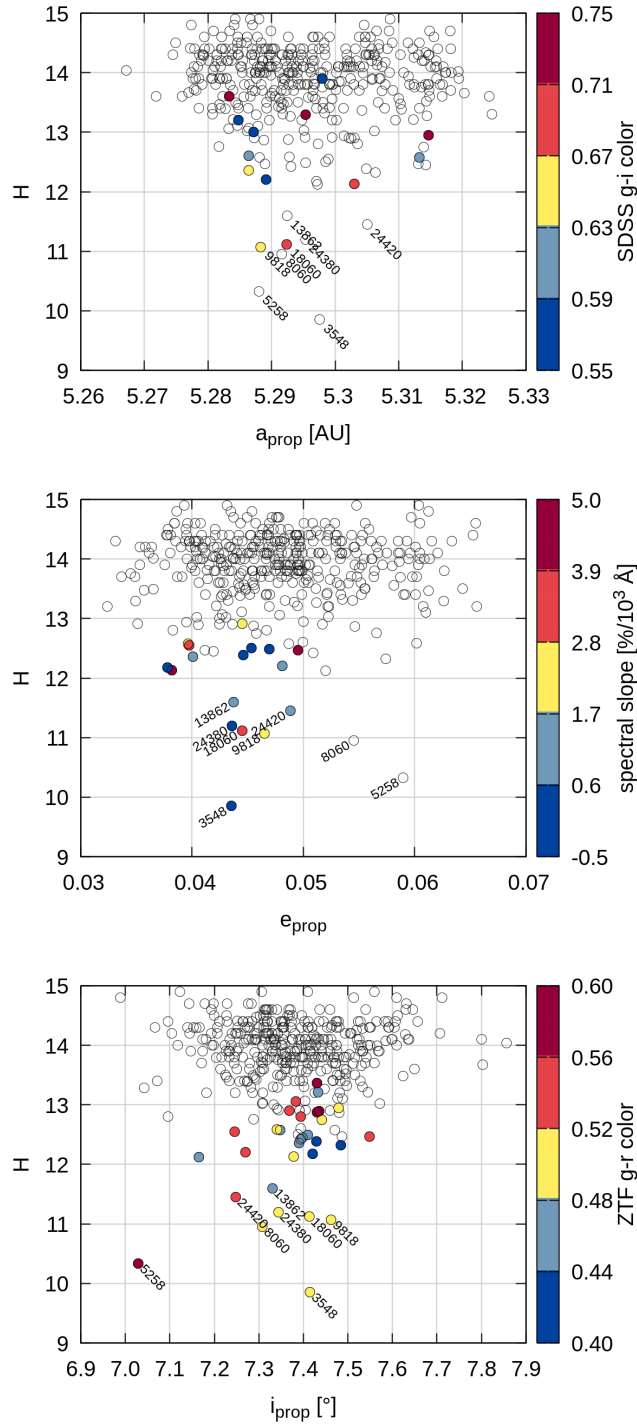


Figure 4: The top panel shows the H-magnitude of the Eurybates family as a function of proper semi-major axis as well as g-i color from the Sloan Digital Sky Survey, SDSS (Ivezić et al., 2001). The text labels indicate the Trojan numbers of the eight brightest family members. The middle panel shows the H-magnitude as a function of proper eccentricity and spectral slope by Fornasier et al. (2007). For direct comparison the color scale has been chosen such that it corresponds roughly to the SDSS color bar in the top panel. The bottom shows the H-magnitude as a function of proper inclination and g-r color from the Zwicky Transient Facility Observations, ZTF (Schemel & Brown, 2021). Trojan (5258) Rhoëo is a clear outlier with respect to proper eccentricity and inclination as well as ZTF color and therefore a very likely interloper. See Table 3 and 4 for all details on the family members depicted here.

low semi-major axis for its size, comparable to (5258) Rhoeo (see top panel in Fig. 4). Other than that, the body is unremarkable with respect to the colors or orbital elements of the other family members. For this reason, we do not consider (9818) Eurymachos an interloper in this work.

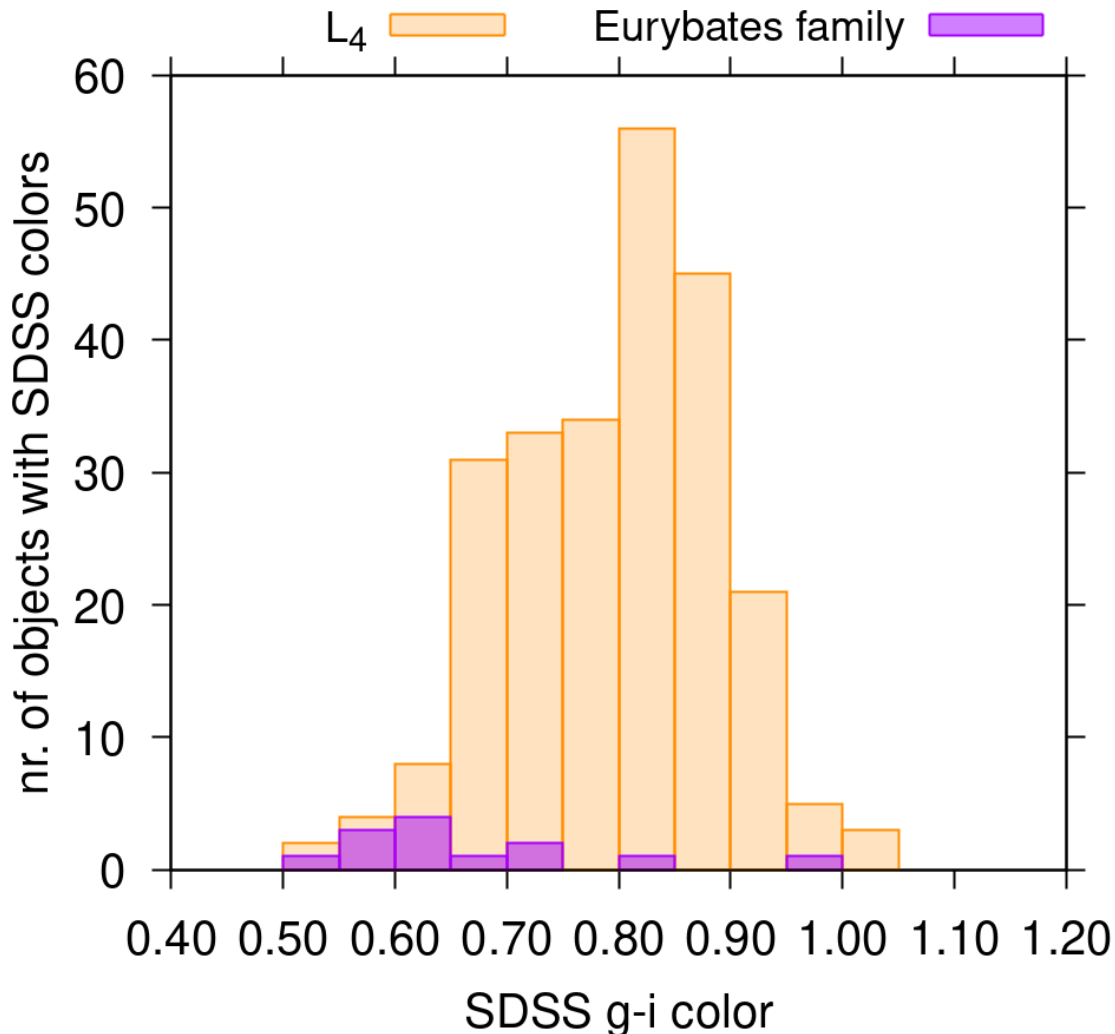


Figure 5: The histogram shows all L_4 Trojans (orange) and all Eurybates family members (purple) with known SDSS colors. The Eurybates family is significantly bluer than the L_4 Trojans overall.

The other larger family members do not have unusual colors or orbital elements. Consequently, for our work here we consider (5258) Rhoeo an interloper and exclude it from what we consider to be the nominal family. The family SFD excluding (5258) Rhoeo is shown in Fig. 3. We can use these data to explore what the SFD tells us about the family forming event.

A substantial amount of work has been done to simulate the outcome of asteroid impacts (e.g. Benz & Asphaug, 1999; Durda et al., 2007; Benavidez et al., 2012; Jutzi, 2015; Benavidez et al., 2018; Jutzi et al., 2019) using primarily a Smoothed Particle Hydrodynamics, SPH, approach. We have access to the simulation results from Durda et al. (2007), who used 100 km diameter monolithic target bodies, and Benavidez et al. (2012), covering collisions of 100 km rubble pile target bodies. Given that these two works cover a large part of parameter space, we consider this to be a good first order reference for possible outcomes.

We used three criteria to determine whether a simulation outcome matched the observed family SFD: 1) the mass ratio of the two largest family members shall be within 25%, 2) the slope between the second and tenth largest object shall be within ± 0.2 , and 3) the slope between the tenth and 30th largest body shall be within ± 0.2 . These criteria were chosen because they fully characterize the

observed family SFD and should so be fairly diagnostic of the family forming collision. For the 387 SPH runs available to us, the mass ratio varied between 3×10^{-5} and 1 (median of 0.03), the slope between the second and tenth largest object varied between -0.6 and -15 (median of -3.7), and the slope between the tenth and 30th largest body varied between -1.6 and -10 (median of -4.4).

We found that only one model outcome out of 387 satisfied all three criteria (see right panel of Fig. 3). The model SFD is remarkably close to the actual family SFD. The simulation corresponded to a collision between a 100 km rubble pile target¹ (Benavidez et al., 2012) and a ~ 35 km impactor ($\log(M_{tar}/M_{imp}) = 1.4$) at 6 km/s and an impact angle of 75° from vertical. Though this match is unlikely to be a unique solution, it is an important piece of information to be evaluated. This is the first indication in our analysis that Jupiter Trojans might be collisionally weak. We will examine this issue below.

A strong constraint for our modeling would be the estimated age of the family, but unfortunately, it is rather poorly constrained. Brož & Rozehnal (2011) and Rozehnal et al. (2016) estimated the family age between 1 and 4 Gy. Milani et al. (2017) was unable to retrieve an age for the Eurybates family from their dynamical methodology. Finally, using the escape probability of family members as derived from dynamical considerations, Holt et al. (2020) estimated the minimum age at $\geq 1.0 \pm 0.4$ Gy. We are hence left at a weak constraint for the family age between 1 Gy and the age of the Solar System.

2.3 Eurybates’ satellite Queta

Our last and arguably most important constraint comes from Eurybates itself. Noll et al. (2020) reported the discovery of a 1.2 ± 0.4 km satellite around (3548) Eurybates, which has since been named Queta. Eurybates is only the fourth Trojan with a known satellite (Noll et al., 2020).

Since its discovery, Queta’s orbit has been further constrained by Hubble Space Telescope observations (Brown et al., 2021). It has a semi-major axis of 2350 ± 11 km, an orbital period of 82.46 ± 0.06 days, and a small eccentricity of 0.125 ± 0.009 (Brown et al., 2021). We find the low eccentricity to be particularly noteworthy because impact simulations (e.g. Durda et al., 2007) typically generate companions around the target body that have highly eccentric orbits. In dynamics, “particles always return to the scene of the perturbation” unless some mechanism has changed their orbit. In Queta’s case this can be due to the Kozai effect which lets Queta’s orbit go through oscillations in eccentricity (Brown et al., 2021).

The existence of Queta as a satellite of Eurybates, the most sizeable member of the largest collisional family within the Jupiter Trojans, immediately poses the question as to the long term survival of Queta. To date, the dynamical stability of Queta has been studied in Brown et al. (2021). Here we will examine whether Queta can survive the expected collisional environment within L_4 . We will summarize the dynamical findings from Brown et al. (2021) in Sec. 3.

3 Methods

To simulate the collisional evolution of the Trojans we employ the *Boulder* collisional code (Morbidelli et al., 2009b; Nesvorný et al., 2011, 2018). Here we only outline the broad principles of the code but a detailed description is provided in Morbidelli et al. (2009b) and Nesvorný et al. (2018). *Boulder* requires an initial SFD of the population, the intrinsic impact probability between bodies (P_i), average impact speeds between bodies, and a function that describes the critical impact energy Q_D^* , defined as the energy per unit target mass needed to disrupt and disperse 50% of the target (e.g. Benz & Asphaug, 1999; Davis et al., 2002). The SFD and P_i are used to calculate the expected number of impacts per time step of the impactor population of size R_i on the targets with size R_j (where $R_i < R_j$). For a given impact *Boulder* calculates the specific impact energy Q , which is defined as the kinetic energy of the impactor divided by the target mass. Collisions where $Q < Q_D^*$ are referred to cratering events while collisions with $Q > Q_D^*$ correspond to super-catastrophic disruption events. When a catastrophic disruption occurs, the code calculates the masses of the largest remnant and that of the largest fragment as well as the power-law slope of the smaller fragments. These values are calculated based on the scaling laws found by the hydrocode results of Durda et al. (2004), Durda

¹Sometimes impact simulation results are scaled to different target sizes to fit family SFDs (e.g. Durda et al., 2004) but this was not needed here.

et al. (2007), and Nesvorný et al. (2006). Each collision alters the SFD which is then used to estimate the subsequent number of expected impacts.

Two fundamental properties of the JTs are unknown: 1) the SFD (in particular for < 10 km) when the Trojans were captured in resonance with Jupiter (we will call this the initial SFD), and 2) the collisional strength of Trojans as defined by Q_D^* . With regards to the initial SFD, our tests suggest collisional evolution will not meaningfully affect the SFD of $D \geq 10$ km Trojans. On this basis, we assume the shape of the Jupiter Trojan SFD for this size range is likely primordial and hence close to the current day SFD. This will also become apparent from our results below. On the other hand the shape of the SFD below 10 km is unknown for the initial population. The present day SFD is complete to ~ 20 km (see Fig. 1) and the slope is arguably well known down to $\sim 3 - 10$ km (Yoshida & Nakamura, 2008; Wong & Brown, 2016; Yoshida & Terai, 2017). We are therefore required to make assumptions about the initial SFD below 10 km. Here we will assume two end member cases. For the first, we will assume that the initial slope below 10 km is simply a continuation of the current day slope above 10 km (2.1, see Fig. 1). For the second, we will assume that the initial slope below 10 km is one ($q = 1$) and thereby significantly shallower than the slope between 10-100 km ($q = 2.1$). This signifies an initial depletion of the JT population at small sizes.

Our version of *Boulder* also allows us to follow the orbital evolution of the Eurybates-Queta system in terms of how impacts on either Eurybates and Queta can alter the orbit of Queta or potentially disrupt either of them (Nesvorný et al., 2011, 2018). Changes to the semi-major axis and eccentricity of Queta are tracked over time. For non-disruptive impacts on either of the binary components, *Boulder* computes the change of the binary orbit depending on the linear momentum of the impactor as described in detail in the methods section of Nesvorný et al. (2018).

We are particularly interested in quantifying the four ways the Eurybates-Queta system can be dissolved: 1) impacts on Eurybates that a) catastrophically disrupt Eurybates or b) displace Eurybates such that Queta is no longer in orbit, and 2) impacts on Queta that a) catastrophically disrupt Queta or b) kick Queta out of orbit. Here we assume a semi-major axis of 2400 km and an eccentricity of 0.1, but we note that the orbit can evolve purely dynamically (Brown et al., 2021). In particular the eccentricity is predicted to oscillate between 0.1 and 0.35 with a roughly 500 year period. This is induced when Queta’s argument of pericenter sweeps by the Kozai resonance islands at 90° and 270° (Brown et al., 2021). We have tested the sensitivity of our results by varying the semi-major axis between 1200 km and 7200 km, and the eccentricity between 0.1 and 0.5. We have not found any significant change of our results within these ranges. For this reason, we will only present the nominal case. But we will return to this point and see why in this case the survival of Queta is not sensitive to the binary semi-major axis.

With regards to Q_D^* we currently do not have a clear sense of the collisional strength of Trojans but can turn to literature for guidance. How impacts disrupt a body depends on the size of the target body, the mass ratio of the target and the impactor, the relative speed and angle of impact, as well as the material properties of the bodies (e.g Holsapple & Housen, 1986; Benz & Asphaug, 1999; Michel et al., 2001; Leinhardt & Stewart, 2009; Jutzi et al., 2010; Benavidez et al., 2012; Holsapple & Housen, 2019; Jutzi et al., 2019).

For the functional form of all Q_D^* we follow the one in Benz & Asphaug (1999) where

$$Q_D^* = C_s \left(\frac{D}{2} \right)^{s_s} + \rho C_g \left(\frac{D}{2} \right)^{s_g} , \quad (2)$$

with D being the diameter of the parent body in cm, ρ the bulk density of the body, and $C_{s,g}$ and $s_{s,g}$ are the scaling constants and slopes in the strength and gravity regimes. Different disruption laws are shown in the left panel of Figure 6. They have primarily been derived for properties suitable to rocky or icy objects. Different techniques have been used to determine Q_D^* . First, numerical models, as e.g. Smoothed Particle Hydrodynamics, SPH (e.g. Benz & Asphaug, 1999; Michel et al., 2001; Jutzi et al., 2010), have been used to simulate the collision of bodies at different impact speeds and angles. Second, models for the collisional evolution of populations (akin to *Boulder*) have been used to constrain the disruption laws by simulating the evolution of the SFD and comparing them with the currently observed SFD in an inverse problem sense (e.g. Bottke et al., 2005, 2020; Benavidez et al., 2022). This method, though it can provide insights into the disruption law of a population, cannot infer material properties on its own. Third, ground truths from laboratory experiments (e.g. Senft & Stewart, 2007, 2008) are crucial to determine the disruption or cratering laws.

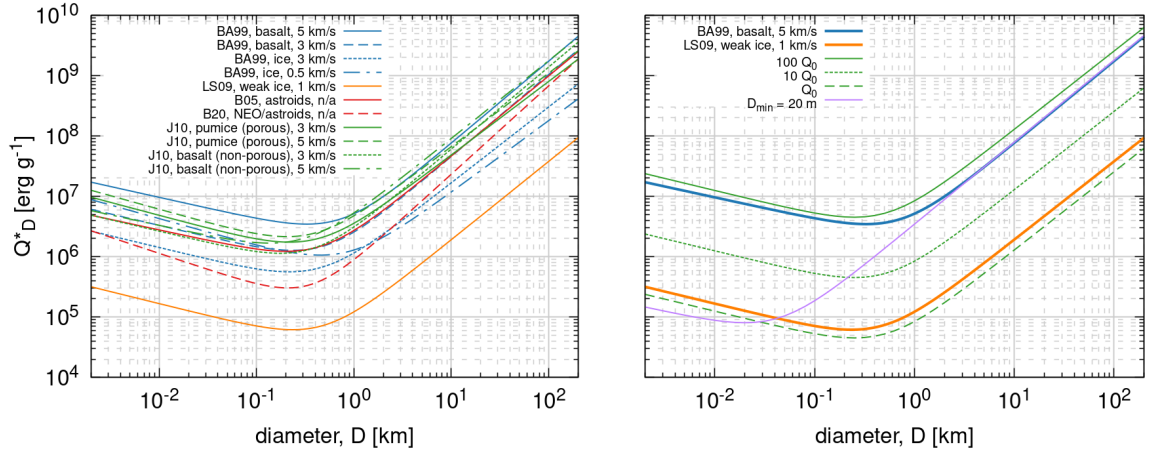


Figure 6: Critical impact energy, Q_D^* , according to different studies (BA99 Benz & Asphaug (1999); LS09 Leinhardt & Stewart (2009); B05 Bottke et al. (2005); B20 Bottke et al. (2020); J10 Jutzi et al. (2010)) are shown in the left panel. The right panel shows three different model assumptions Q_0 (dashed green), $10Q_0$ (dotted green), and $100Q_0$ (solid green) as well as a Q_D^* with a minimum at 20 m (purple line). In addition the literature values from Benz & Asphaug (1999) (blue) and Leinhardt & Stewart (2009) (orange) are shown as a reference. This illustrates that our weakest material (Q_0) is slightly weaker than the weak ice from Leinhardt & Stewart (2009) while our strongest material ($100Q_0$) is slightly stronger than the basaltic material from Benz & Asphaug (1999).

The Q_D^* illustrated in Figure 6 show many common features. They all have a minimum at a similar size of $D_{min} \in [200, 400]$ m. This divides the curves into the so-called gravity regime (to the right of the minimum) and the strength regime (to the left of the minimum). The slopes in both the gravity and strength regime do not vary strongly. Lastly, despite the similarity in shape, the Q_D^* functions vary significantly in absolute strength. The weak ice material of Leinhardt & Stewart (2009) (orange line in Fig. 6) is almost two orders of magnitude weaker than the basaltic material in Benz & Asphaug (1999) (blue line in Fig. 6).

We have for this reason chosen to retain the canonical shape of Q_D^* and vary only the magnitude over two orders of magnitude. Our weakest material will be denoted by Q_0 (see right panel of Fig. 6) and corresponds to materials slightly weaker than the weak ice from Leinhardt & Stewart (2009). We then include scaling of $2.2Q_0$, $4.6Q_0$, $10Q_0$, $22Q_0$, $46Q_0$, and $100Q_0$ where the latter is slightly stronger than the basaltic material from Benz & Asphaug (1999). Given the match in the family SFD with the runs of Benavidez et al. (2012) (Fig. 3), the strength of Proto-Eurybates would correspond to our $4.6Q_0$ case.

Finally, we will also consider a more exotic Q_D^* (purple line in right panel of Fig. 6) which follows the basaltic material from Benz & Asphaug (1999) in the gravity regime but then continues down to $D_{min} = 20$ m before transitioning to the strength regime. We will discuss the motivation and implications for this kind of Q_D^* in Sec. 4.

3.1 Input parameters

In the previous section, we have mentioned the input parameters that are needed for this work. First, we have described that the *Boulder* code requires population-specific parameters. These are the initial SFD, intrinsic impact probability, P_i , and the average impact speeds, v_i , of the population. In the case of the JTs we can treat the two swarm separately because they do not overlap dynamically and thus do not contribute to the collisional evolution of each other. For the SFD we, therefore, assume a slightly larger population than L_4 . The largest object in our SFD has a diameter of 140 km. Between our largest size and 100 km we have a steep slope leading to 15 Trojans larger than 100 km. Below 100 km we impose a cumulative slope of 2.1 down to our smallest size of 2 m. This initial SFD is shown in later figures (e.g. Fig. 10) and has a total mass of $4 \times 10^{-6} M_{\oplus}$. This mass is consistent with the estimate by Nesvorný et al. (2013). The collisional environment within each swarm is defined by $P_i = 7 \times 10^{-18} \text{ km}^{-2} \text{ yr}^{-1}$ and $v_i = 4.6 \text{ km s}^{-1}$ (Davis et al., 2002; Nesvorný et al., 2018). The

Table 1: Parameters used for Q_D^* in this work, and resulting minimum of Q_D^* , D_{min} .

C_s [erg g ⁻¹]	s_s	C_g [erg cm ³ g ⁻²]	s_g	ρ [g cm ⁻³]	D_{min} [m]	description
1.50×10^6	-0.40	0.05	1.30	1	250	Q_0 case
7.65×10^5	-0.36	1.40	1.36	1	20	Q_D^* with minimum at 20 m

intrinsic impact probability takes into account the resonant dynamics of the Trojans.

The second set of input parameters relates to the material properties of the JTs through the Q_D^* . As described above we have tested two types of disruption laws, one with a canonical shape and a minimum in Q_D^* at $D = 250$ m and one with a minimum at $D = 20$ m. The former Q_D^* form a set with the weakest material labeled Q_0 . Scaled versions of Q_0 have been tested up to $100 \times Q_0$ (see Fig. 6). The parameters Q_D^* (Eq. 2) used in this work are listed in Table 1.

4 Results

There are essentially three unknowns in our simulations as defined above: 1) the initial Jupiter Trojan SFD below 10 km; 2) the collisional strength of JTs, Q_D^* ; and 3) the age of the Eurybates family. Here we present our results that will illustrate how these three properties affect each other, and what we can learn about them. With respect to the age of the Eurybates family, we stipulate that this is equal to the age of Queta, thereby assuming that Queta formed during the family forming collision. While this is not necessarily true we are of the opinion that this is a sound assumption absent any other data. As a result we use the age of the family and Queta interchangeably.

To keep things simple, we first start with a simplified situation of a static Jupiter Trojan SFD and will then add more complexity by allowing the SFD to collisionally grind down over time. Finally, we present the results for a non-canonical Q_D^* which might have interesting implications for other small body populations in the outer Solar System.

4.1 Static SFD

In a first step we assume that the SFD of the JT population has not evolved over the age of the Solar System. To do this we switch off the collisional evolution of the SFD in *Boulder*. This retains only the part of the code that monitors impacts on the Eurybates-Queta system and as a consequence allows us to separate the effects from the evolving Trojan SFD (see next section) and the inherent survival probability of Queta given a certain Trojan population. Though this is a simplification it does allow us to retrieve a first estimate for the time scales. As described above we assume two different initial SFDs.

First, we assume that the SFD below 10 km continues with the same slope as at larger sizes (2.1, see orange line in Fig. 10). In this case the probability that Queta survives is a simple exponential decay over time and depends only on Q_D^* (left panel of Fig. 7). At a certain age of the family the probability that Queta would have survived to this day becomes so small that we should not consider these cases. For our purpose we use a 10% survival probability as a discriminator between a scenario which we still consider plausible and scenarios where it would simply be too unlikely for Queta to have survived. We find that a large part of parameter space can be excluded (right panel of Fig. 7).

Therefore, Figure 7 can answer the question of the age of the Eurybates family as a function of collisional strength. Any cases below the 10% contour line in the right panel of Fig. 7 should be considered statistically improbable. Given this static SFD with a slope of 2.1 between 2 m and 100 km, we find that Q_D^* needs to be strictly larger than $4.6Q_0$. Otherwise Queta would not survive for more than 1 Gy, the lower limit for the family age. Interestingly, $4.6Q_0$ corresponds to the Q_D^* found by Benavidez et al. (2018) for their rubble pile asteroids. As we have seen above, one of their simulations is a good fit to the SFD of the Eurybates family. If the parent body of the Eurybates family was indeed this weak ($4.6Q_0$), and this disruption law is representative of Jupiter Trojans, and the current day SFD continues with the same slope down to small sizes, then this result would suggest that the Eurybates family is a “young” family (1 Gy).

We also observe that the age of the family and the collisional strength are directly linked. As the

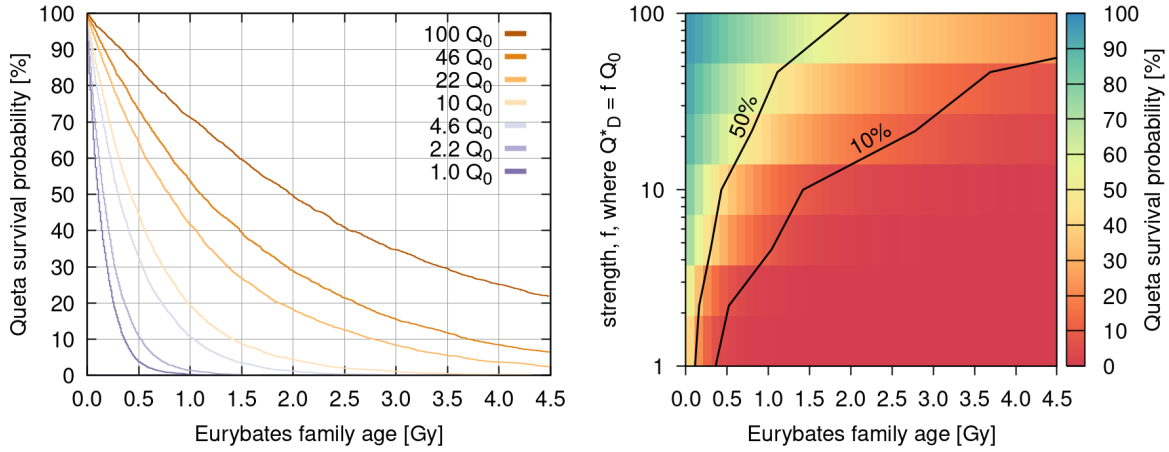


Figure 7: The left panel shows the survival probability of Queta as a function of the family age for the different Q_D^* of our study. The right panel shows the same information but as a function of collisional strength. The two black lines show the 10% and 50% survival contours. Cases below the 10% contour should be discarded as viable cases. For these cases a static SFD with a cumulative slope of 2.1 between 2 m and 100 km was assumed.

collisional strength increases so does the age of the family. Strictly speaking these are all upper limits for the age of the family. For example, our strongest material ($100Q_0$) never falls below 10% and hence the family age could be up to the age of the solar system. On the other hand the $46Q_0$ case, which in fact corresponds roughly to the Q_D^* of basaltic material in Benz & Asphaug (1999) (see blue line in Fig. 6) gives us an upper limit of ~ 3.7 Gy for the family age.

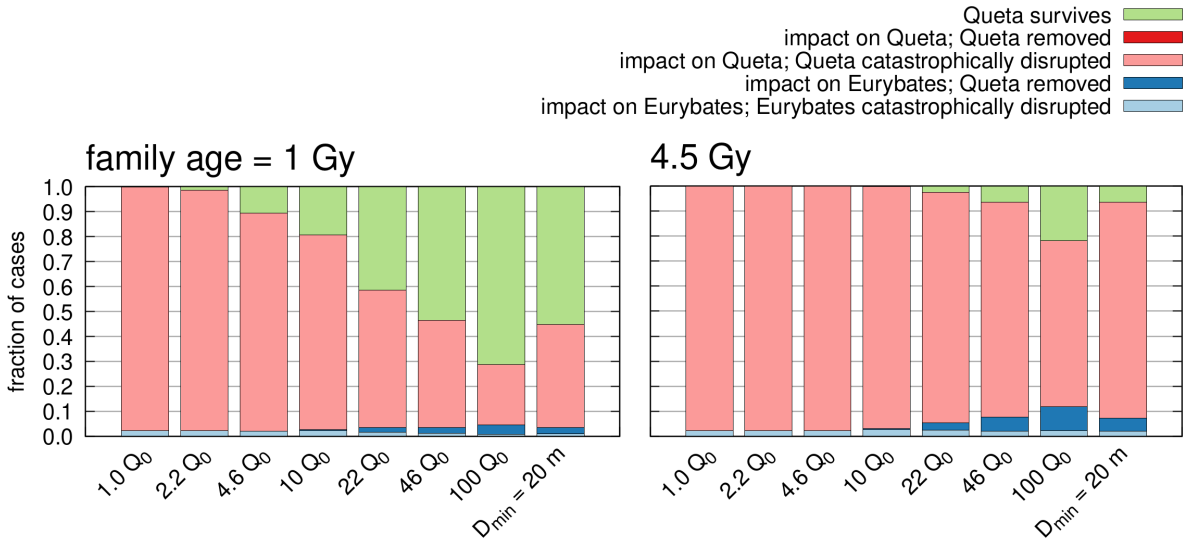


Figure 8: The fraction of outcomes for the Eurybates-Queta system are shown for a family age of 1 Gy (left panel), and 4.5 Gy (right panel). A static SFD with a slope of 2.1 between 2 m and 100 km (section 4.1) is assumed here.). A total of 1000 runs were performed to estimate the fraction of outcomes of each case.

We can also examine what contributes to the destruction of the Eurybates-Queta system. Fig. 8 shows our results for different Q_D^* and a family age of 1 Gy (left) and 4.5 Gy (right). We find that in the overwhelming fraction of cases, an impact occurs on Queta that catastrophically disrupts it (pink in Fig. 8). There are no cases where an impact on Queta perturbs its orbit enough for the binary to be dissolved (red in Fig. 8). In a minor fraction of cases (up to 10% after 4.5 Gy for $100Q_0$), an impact on Eurybates leads to the ejection of Queta. It is interesting to note that the relative fraction

of cases where an impact on Eurybates destroys Eurybates (light blue in Fig. 8) decreases with respect to when such an impact dissolves the binary (dark blue in Fig. 8). This result makes sense because as the material strength increases it becomes harder to catastrophically disrupt Eurybates but “easier” to nudge Eurybates such that the binary orbit is dissolved and Queta lost from the system. The fact that the survival of Eurybates-Queta system is dominated by impacts on Queta is noteworthy because it is different than what has been observed for other binaries, in particular the large Trojan binary pair of Patroclus and Menoetius (P-M binary; Nesvorný et al., 2018), the final fly-by target of the Lucy mission. The P-M system is an almost equal size binary with diameters of 113 km and 104 km respectively. The survival of the P-M binary is limited by impacts on one of the components that alter the orbit such that the binary is dissolved. The binaries survival is thus sensitive to the semi-major axis of the binary (Nesvorný et al., 2018) because binaries with larger semi-major axis are dissolved more easily than tight binaries. Nesvorný et al. (2018) estimated that the specific energy needed to dissolve the P-M binary through a non-catastrophic impact is much smaller than the respective Q_D^* . In our case, it is much easier to catastrophically disrupt the much smaller Queta (~ 1 km). Therefore, in contrast to the P-M binary, the Eurybates-Queta system’s survival is not sensitive to the semi-major axis.

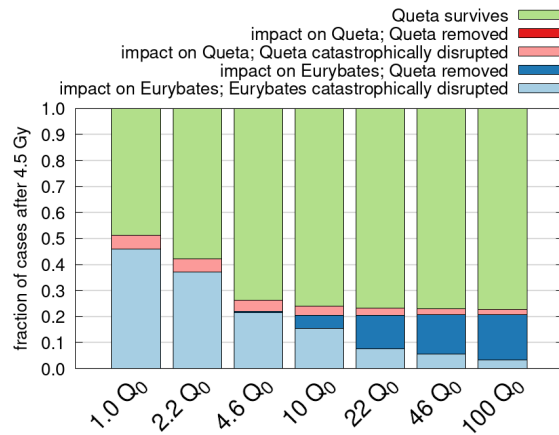


Figure 9: The fraction of outcomes for the Eurybates-Queta system are shown for a family age of 4.5 Gy when the initial Jupiter Trojan SFD is shallow (power law of 1) below 10 km.

Up to now we have assumed that the Jupiter Trojan SFD simply continues below 10 km with respect to the slope above 10 km. Because there are indications that the SFD bends/breaks at or somewhat below 1 km (Yoshida & Nakamura, 2008; Wong & Brown, 2015; Yoshida & Terai, 2017), we now assume that the Trojan SFD has a break at 10 km and continues at small sizes with a slope of $q = 1$ (significantly flatter than above 10 km). In this case, we find a very different picture to the one above (Fig. 9). We find that the age and collisional strength become unconstrained. Queta can survive 4.5 Gy in all cases of Q_D^* . In the worst case scenario with extremely weak material (Q_0) there is still a 50/50 chance of Queta surviving. In most cases ($Q_D^* \geq 4.6Q_0$) the survival probability of Queta over 4.5 Gy is $\sim 80\%$.

This behavior is readily explained. Due to the very flat SFD below 1 km, the impactor population that could destroy Queta is simply not very large. Consequently the probability for Queta to be catastrophically disrupted (pink in Fig. 8 and 9) shrinks to the single percent digits. In this situation, the probability of the Eurybates-Queta system being disrupted is dominated by impacts on Eurybates. This happens either by direct disruption of Eurybates in the case of weak material or dissolution of the binary for strong material. Further, we observe a transition from disruptions of Eurybates dominating the survival probability at low collisional strength to impacts on Eurybates dissolving the binary at large collisional strengths. At low strength, Eurybates is easily disrupted and thus becomes the primary mode limiting the retention of Eurybates-Queta system. As the strength increases Eurybates becomes hard to disrupt but can be nudged strongly enough to dissolve the orbit of Queta.

4.2 Evolving SFD

As argued above the assumption of a static Jupiter Trojan SFD over the age of the Solar System is likely to be an unrealistic simplification. Accordingly, we now consider an initial Trojan SFD with a slope of 2.1 below 10 km (see orange line in Fig. 10) and let it evolve over the age of the Solar System. The results of 300 such simulations for a Q_D^* of Q_0 and $100Q_0$ are shown in Figure 10. We show 300

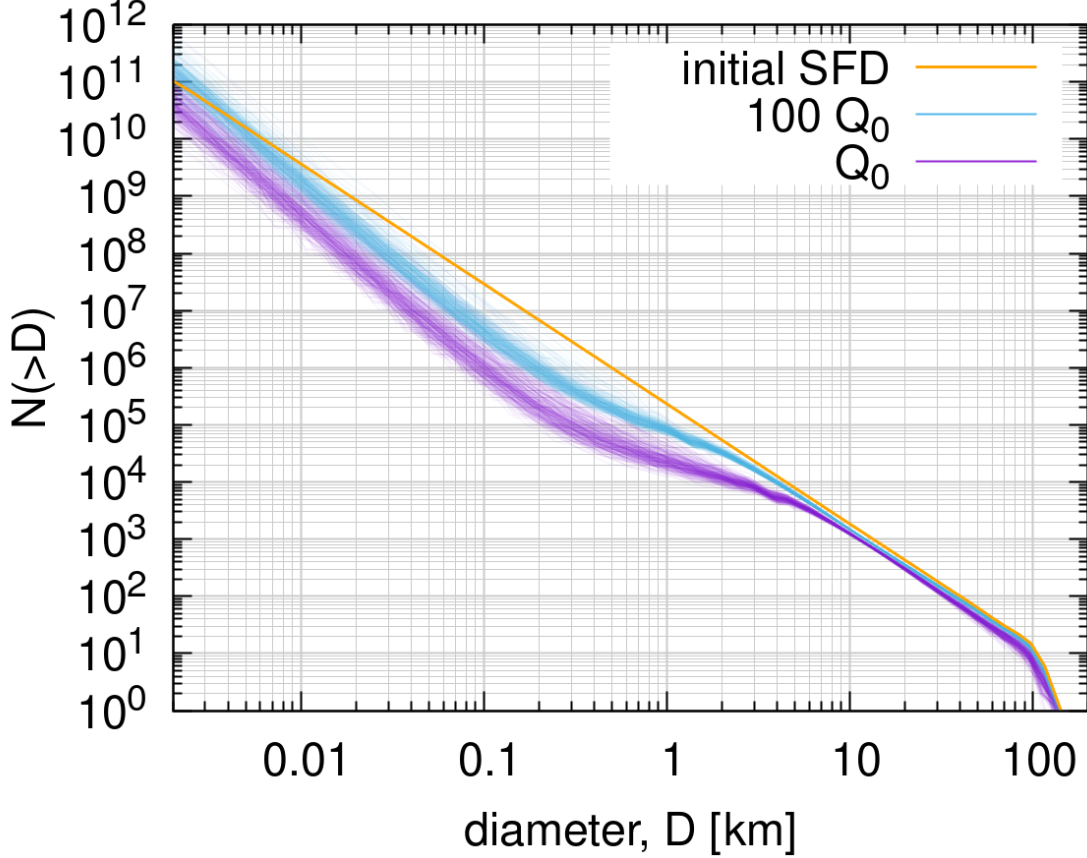


Figure 10: The initial Trojan SFD is shown in orange. The faint lines in purple are 300 different SFDs after 4.5 Gy of collisional grinding assuming $Q_D^* = Q_0$ while the blue lines assume $Q_D^* = 100Q_0$.

simulations to illustrate the stochastic nature of the collisional evolution of the Trojan population. The sets of simulations differ only in the random seed given to the code. Each simulation, therefore, signifies a possible future of the same initial state of the system.

We find that the slope between ~ 6 km and 100 km remains unaltered though the population is depleted slightly in both cases. In both cases shown in Fig. 10 the SFD below ~ 6 km is significantly affected by collisional grinding. In particular, the population is depleted between 10 m and 3 km. This results in a turnover between 2 and 6 km. The location of this bend depends on the Q_D^* . It is likely that this is the cause of the bend in the SFD seen by [Yoshida & Nakamura \(2008\)](#) and [Wong & Brown \(2015\)](#). But we should also point out that [Yoshida & Terai \(2017\)](#) reported no detection of this bend and thus its existence and location requires further observations. From a theoretical standpoint we expect there to be a bend in the Trojan SFD (Fig. 10) therefore it is likely “merely” a matter of getting more observations to identify it.

The depletion of the JT population between 10 m and 1 km directly affects the survival probability of Queta because this is the impactor population responsible for its destruction (see above). We find that the survival probability of Queta significantly increases in all cases (see bottom row of Fig. 11). Compared to the static SFD (Fig. 8), all of the Q_D^* allow Queta to plausibly survive with a family age of more than 1 Gy. But for these cases, we also need a material strength of at least $10Q_0$ for Queta to have a 10% chance of surviving the age of the Solar System.

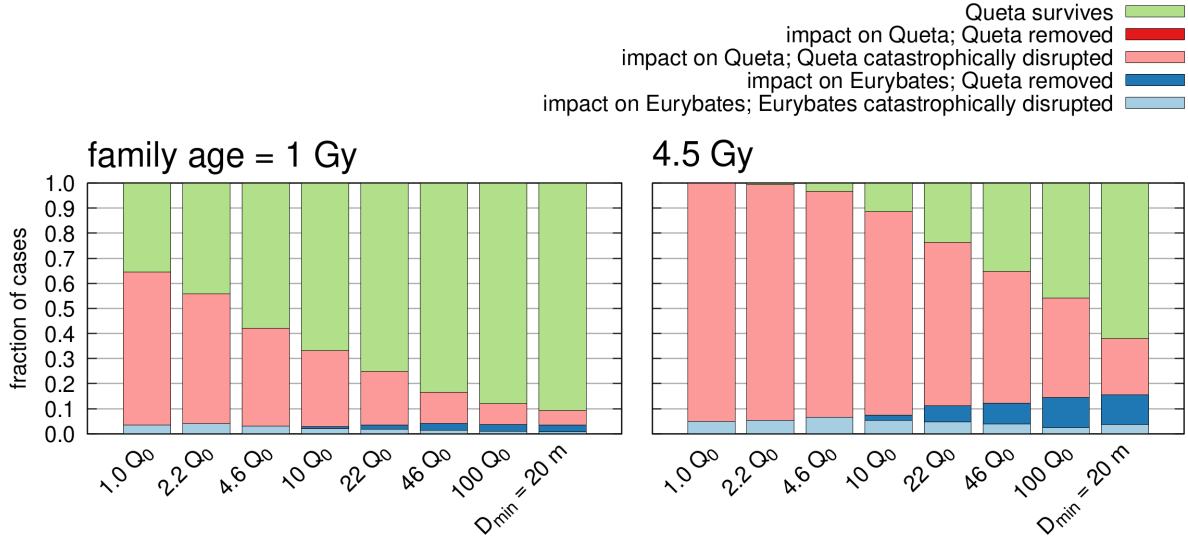


Figure 11: The fraction of outcomes for the Eurybates-Queta system are shown for a family age of 1 Gy (left panel), and 4.5 Gy (right panel). The results here take into account the changing SFD due to collisional grinding (section 4.2). A total of 1000 runs were performed to estimate the fraction of outcomes of each case. FIGURE WAS SPLIT FROM FIG. 8.

Figure 12 shows the survival probability as a function of the family age. Compared to the static SFD (Fig. 7) we observe that the decay is no longer exponential but becomes almost linear in time for the strongest material. Further, the part of parameter space consistent with Queta’s existence (cases above the 10% contour) is greatly expanded compared to the static SFD (right panel of Fig. 7). This result is not a surprise because there are fewer projectiles in the population capable of destroying Queta. The collisional strength derived for the [Benavidez et al. \(2012\)](#) rubble piles with $Q_D^* = 4.6Q_0$ now puts an upper limit on the family age. The family is no older than 3.7 Gy with a probability of 90% for this size distribution and disruption law.

4.3 Unconventional Q_D^*

Finally, we will examine what happens to our results if we employ a more unconventional Q_D^* . As described in section 4.2 (see also Fig. 6) the minimum value of Q_D^* in literature for rocky and icy targets is typically around a diameter of $D_{min} = 200$ m. There are indications from cratering results obtained by the New Horizons mission to the Pluto system and to the cold classical KBO Arrokoth ([Singer et al., 2019](#); [Morbidelli et al., 2021](#)), however, that this might not hold for icy bodies of the outer Solar System. The critical clue is that the cumulative power law slope of the Kuiper belt SFD is approximately $q = 1$ over the size range between 1 km and tens of meters in diameter [Morbidelli et al. \(2021\)](#).

As discussed in section 4.2, the location where the intermediate slope steepens back up to the slope in the strength regime is indicative of the minimum in Q_D^* . For the asteroid belt, this change in slope is observed at 200 m (e.g. [Bottke et al., 2020](#)). For the Kuiper belt, we have yet to identify the size of where this putative change in slope would take place. All we can say is that if it exists, it has to occur at sizes smaller than tens of meters. Accordingly, we infer that Q_D^* for Kuiper belt objects, and presumably Trojans, need to have a minimum value smaller than a few tens of meters. We therefore assume an unconventional Q_D^* (purple line in right panel of Fig. 6) which follows the [Benz & Asphaug \(1999\)](#) basaltic material in the gravity regime but then continues down to include continuously weaker material strength all the way down to $D_{min} = 20$ m before transitioning to the strength regime. This minimum value is consistent with the arguments made by [Morbidelli et al. \(2021\)](#), namely that a upturn near that point would provide the means to explain the quantity of dust observed in the Edgeworth-Kuiper belt by New Horizons.

Figure 13 shows what the SFD evolved to after 4.5 Gy. The SFD is more complex than the ones previously shown (Fig. 10). We interpret it using the local slopes shown in the right panel. Here we

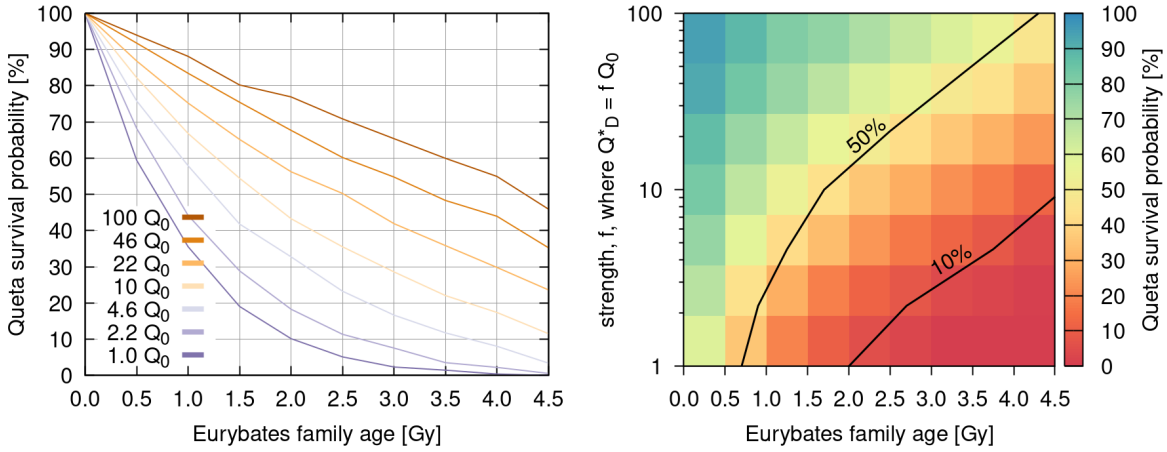


Figure 12: The left panel shows the survival probability of Queta for the evolving Trojan SFD case as a function of the family age for the different Q_D^* of our study. The right panel shows the same information but as a function of collisional strength. The two black lines show the 10% and 50% survival contours. Cases below the 10% contour should be discarded as viable cases.

have defined the local slope as the power law index connecting the two adjacent size bins within the Boulder output results. The typical distance between size bins is $1.25D$.

O’Brien & Greenberg (2003) showed for a population in collisional equilibrium that the differential power law exponent, p , is connected to the slope, s , of the gravity or strength regime respectively via:

$$p = \frac{7 + |s|}{2 + |s|} . \quad (3)$$

If Q_D^* is independent of size (i.e. $s = 0$) we retrieve the classical Dohnanyi steady-state solution of $p = 3.5$ (Dohnanyi, 1969). In our case the gravity regime of Q_D^* has a slope of $s = 1.3$ resulting in $p = 3.05$ which corresponds to a cumulative slope of 2.05. This is close to the observed slope between 10 and 100 km which could indicate that this part of the population was in collisional equilibrium when the Trojans were captured. The slope at small sizes should correspond to the respective slope predicted for the strength regime. In between the two steep slopes at the very small and large sizes we find a shallow slope in the diameter range from roughly 30 m to 1 km. Note that the location where the SFD transitions to the slope in the strength regime is precisely the location of the minimum in Q_D^* at roughly $D_{min} = 100 - 200$ m of the traditionally shaped Q_D^* (Fig. 10), and $D_{min} = 20$ m for our unconventional Q_D^* (Fig. 13). This makes sense as objects smaller than D_{min} are stronger than their larger companions. As a consequence they can more easily break larger objects but not be easily broken up themselves.

Starting at large JTs ($10 \text{ km} < D < 100 \text{ km}$) in Fig. 13, the SFD is largely unchanged from the initial SFD, and retains $q \sim 2$. Few of these objects have disrupted. At 10 km the slope begins to steepen slightly reaching a peak at around 2.5 km before beginning to flatten. This indicates a steady state “bump” is being formed by collisional evolution; it is analogous to the bump seen in the asteroid belt near 2-3 km, and we will discuss its origin below. The flattest part of the SFD occurs at ~ 200 m. From there the slope steepens up again to reach the predicted slope in the strength regime for a collisionally-evolved Dohnanyi-like SFD (O’Brien & Greenberg, 2003). This final slope is reached as expected around $D_{min} = 20$ m. As with the asteroid belt, the limited number of projectiles near this minimum means there should be an excess of bodies at larger sizes corresponding to the targets that would be disrupted by 20 m projectiles. That explains the change of the aforementioned “bump” at around 1 km. Similarly, the slight “dip” in the population around 10 km is produced by the excess number of 1 km bodies in the bump. Intriguingly, there may be some limited evidence of a “dip” near 10 km Trojans. The tentative shallowing of the slope at small sizes (~ 5 km Yoshida & Nakamura, 2008; Wong & Brown, 2015) is associated with a slightly steeper slope than the nominal 2.1 just before the apparent turn over. While this is not definitive proof, and details need to be worked out in future work and observations, we argue that there is sufficient support here to warrant seriously entertaining the possibility of an unorthodox Q_D^* with a D_{min} at ~ 20 m.

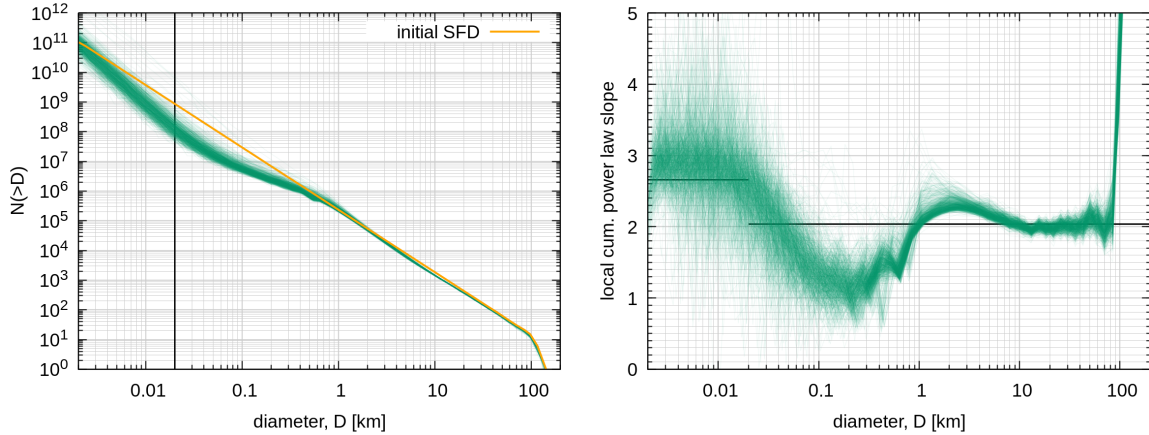


Figure 13: The left panel shows the evolved SFDs after 4.5 Gy assuming a Q_D^* with $D_{min} = 20$ m. For reference the initial SFD is shown in orange. The right panel shows the slopes assuming a local power law as well as the theoretical slopes (solid black) given by Eq. 3. Both the largest and smallest Trojans approach the predicted slopes. The intermediate size regime shows a mild wave of the SFD which steepens up between 1-10 km before becoming shallow below 1 km and finally converging to the strength regime slope.

It is also worth mentioning that the bump at ~ 1 km can cause the current day population to exceed the initial population at that size (left panel of Fig. 13). This is not observed in any of the cases that use a traditionally-shaped Q_D^* . The reason is that traditionally shaped Q_D^* produce a turnover at larger sizes (3-7 km) than for our unconventional Q_D^* (below 1 km). This leads to a smaller 1 km impactor population for traditional Q_D^* functions that is not large enough to disrupt many Trojans of the order of 10 km, i.e., it cannot produce a dip at those sizes. These larger breakups act as a source population for further 1 km Trojans and, therefore, allow a “bump” in the unconventional Q_D^* case.

This model not only has the advantage of fitting into the data returned by the New Horizons mission (Singer et al., 2019; Morbidelli et al., 2021) and qualitatively matching the flattening of the Jupiter Trojan SFD at small sizes (Yoshida & Nakamura, 2008; Wong & Brown, 2015) but it also liberates the constraint on the collisional lifetime of Queta and thus the age of the Eurybates family.

In fact, this unconventional Q_D^* would allow Queta to survive under any of our assumptions for at least the age of the Solar System (Figs. 8 and 11). The reason is that the projectile population capable of disrupting Queta is low and stays that way for 4.5 Gyr.

This unconventional Q_D^* , though, would not match the strength of Proto-Eurybates derived from SPH simulations in Sec. 2.2. Note also that we have tested smaller values for D_{min} , but they produce SFDs that are less consistent with New Horizons crater constraints because the shallow slope in the SFD continues to even smaller sizes than shown in Fig. 13. This would make it difficult to reconcile the New Horizons crater record with the Kuiper belt dust observations (see argument in Morbidelli et al., 2021).

5 Discussion

The main avenue for disrupting the Eurybates-Queta system is via direct impacts on Queta (Figs. 8 and 11). Thus the crucial factor in the survival of Queta is the impactor population below 1 km. For Queta to survive from its creation in the Eurybates family forming impact to today and not have its survival be a fluke, we need to limit the number of projectiles that can disrupt Queta. From a collisional evolution perspective, that means the slope of the Jupiter Trojan SFD below 1 km needs to be shallow. This can be achieved by material with a traditionally shaped Q_D^* or a more unorthodox shaped Q_D^* that has a minimum at 20 m.

In the first case, not all Q_D^* functions allow Queta to survive the age of the Solar System. If the collisional strength is too low, Queta is too easily disrupted, even though the Trojan SFD collisionally grinds down a substantial amount. For these kinds of runs, a minimum of $10Q_0$ is needed for the

Table 2: Minimum number of expected craters on Eurybates, N_C , accumulated during 2 Gy which are larger than a certain diameter for different Q_D^* . This calculation does not take into account saturation.

Q_D^*	$N_C(> 1 \text{ km})$	$N_C(> 10 \text{ km})$	$\frac{N_C(>1 \text{ km})}{N_C(>10 \text{ km})}$
Q_0	200	4	50
$100Q_0$	800	16	50
$D_{min} = 20 \text{ m}$	1200	50	24

long term (i.e. the age of the Solar System) survival of Queta. The problem is that this value is inconsistent with the inferred strength against disruption we have found for Eurybates based on the family SFD ($4.6Q_0$; Fig. 3) derived from the SPH family forming impact simulation. If, on the other hand, we relax the condition that the family be as old as 4.5 Gy and instead insist that $Q_D^* = 4.6Q_0$ then there is a 90% chance that the family is no older than 3.7 Gy (Fig. 12). Thus for a traditional Q_D^* , either, the family is likely younger than the age of the Solar System, or the collisional strength of Proto-Eurybates ($4.6Q_0$) was lower than the overall Trojan population ($> 10Q_0$).

The case of a traditionally shaped $Q_D^* \leq 4.6Q_0$ leads to a high probability that Queta experiences a catastrophic impact during the lifetime of the Solar System. For Queta to still survive in such a scenario would require an additional mechanism. It is imaginable that Queta re-accumulated after a catastrophic disruption event, or that Queta was initially much larger than today and has undergone significant collisional grinding since. The latter, in particular, seems unlikely as impact simulations primarily result in small satellites (e.g. Durda et al., 2004). The existence of small satellites also seems consistent with observed satellites in the main belt (e.g. Fig. 4 in Noll et al., 2020).

In the second case, with an unconventional shaped Q_D^* that has its minimum at 20 m, Queta can easily survive the age of the Solar System and, therefore, the Eurybates family can be as old as 4.5 Gy. But, again, this would bring the collisional strength of Proto-Eurybates and the overall Trojan population into disagreement.

The fact that several Q_D^* are consistent with the survival of Queta, raises the question as to how we shall distinguish these cases. Figures 10 and 13 show that the Jupiter Trojan SFD can evolve to very different shapes when a variety of Q_D^* functions are used. This result has direct consequences for the expected crater SFD that the Lucy mission will observe. A back of the envelope estimate shows that these contrasting Trojan SFDs lead to a stark differences in the expected number of craters forming on a Trojan over a given amount of time, e.g., Eurybates (Table 2). For the purpose of this estimate, we assume a crater to impactor ratio of 10 (e.g. Singer et al., 2019) (e.g. a 1 km impactor would produce a 10 km crater). As Table 2 illustrates the number of craters on Eurybates increases by a factor of four when the collisional strength increases from Q_0 to $100Q_0$. The fact that our unconventional Q_D^* results in the largest number of craters seems counterintuitive at first but Figs. 10 and 13 hold the answer. Because the shallow part of the Trojan SFD occurs at smaller sizes for the unconventional Q_D^* compared to the traditionally shaped Q_D^* , the overall population at sizes between 100 m and 1 km, corresponding to a projectile size range between 10 m and 100 m, is larger. This outcome leads to more craters. Additionally, the case of our unconventional Q_D^* likely leads to a saturated cratered surface, potentially complicating how our crater SFDs will be linked to the impactor SFD. Furthermore, the ratio between the number of craters larger than 1 km and 10 km is different for the case of our unconventional Q_D^* compared to the traditionally shaped Q_D^* with the latter producing more small craters for every large crater. In the case of traditionally shaped Q_D^* the slope of the Trojan SFD increases at roughly 300 m while for the unconventional Q_D^* the slope remains flat between 60 m and 1 km. This results in the different ratios of large to small impacts. Lucy, being able to measure craters as small as 70 m, and therefore sensitive to projectile sizes as small as 7 m, will be able to determine the crater SFD to sufficient precision to potentially differentiate between these case studies, assuming the surfaces are not saturated. In turn, this would allow us to indirectly estimate the collisional strength of the Trojans and the Q_D^* disruption law followed by both Trojans and similar objects.

6 Summary & Conclusions

In this work we have modeled the collisional evolution of the Jupiter Trojans and determined under which conditions the Eurybates-Queta system survives. We have shown that the collisional strength

of the Jupiter Trojans and the age of the Eurybates family and Queta are correlated. This correlation depends itself on the initial Trojan SFD and how it collisionally evolves over time.

We found that the Eurybates family SFD matches best the outcome of SPH models of a 100 km rubble pile target (Benavidez et al., 2012) being hit by a ~ 35 km impactor ($\log(M_{tar}/M_{imp}) = 1.4$) at 6 km/s, and an impact angle of 75° . This corresponds to objects with a collisional strength of $Q_D^* = 4.6Q_0$, where Q_0 corresponds to slightly weaker material than the “weak ice” from Leinhardt & Stewart (2009).

In the case of static SFDs that don’t evolve over time we examined a nominal case where the Jupiter Trojan SFD at small sizes (< 10 km) has the same slope as between 10-100 km. With this SFD, and assuming the parent body of the Eurybates family was indeed weak, and is representative of Jupiter Trojans, we found that the Eurybates family must be a “young” family (1 Gy).

Should the Trojan SFD have break at 1 km and have a shallow slope below that break then we cannot constrain the age of the Eurybates family and collisional strength of the Trojans. The slope of the SFD below 1 km is the driving property to assess the family age and collisional strength. This is due to the fact that the population between 10 m and 1 km is the impactor population which can disrupt Eurybates and Queta.

Further, we found that the collisional grinding of the JT population results in a SFD that remains largely unaltered at large sizes (> 10 km) but is then depleted at intermediate small sizes (10 m to 1 km). This implies a turn over in the SFD, the location of which depends on the Q_D^* . It is to be expected that the Trojan SFD bends towards a shallower slope between 1 and 10 km (Yoshida & Nakamura, 2008; Wong & Brown, 2015; Yoshida & Terai, 2017).

For more realistic cases where the Trojan population is allowed to collisionally evolve we find the following: A material strength of at least $10Q_0$ is needed for Queta to survive the age of the Solar System. For the likely strength of Eurybates ($4.6Q_0$) there is a 90% chance that the family cannot be older than 3.7 Gy.

We find that an unconventional Q_D^* with a minimum at $D_{min} = 20$ m is a plausible candidate that does not require any additional assumptions on the Trojan SFD or age of the Eurybates family. Further, it fits into the data returned by the New Horizons mission (Singer et al., 2019; Morbidelli et al., 2021) for the craters on Charon and KBO Arrokoth as well as the qualitative behavior of the Jupiter Trojan SFD at small sizes (Yoshida & Nakamura, 2008; Wong & Brown, 2015).

Finally, we have shown how different Q_D^* will impact the expected number of craters on the targets of the Lucy mission. The data from Lucy may be able to differentiate between different cases of Q_D^* and subsequently indirectly determine the collisional strength of Jupiter Trojans.

7 Appendix

Table 3: List of all 400 Eurybates family members identified by the hierarchical clustering method (HCM) including the likely interloper (5258) Rhoeo (see discussion in Sec. 2). The table gives the asteroid number (#), the provisional designation (prov. des.), the absolute magnitude (H), the diameter (D), as well as the proper semi-major axis (a_{prop}), eccentricity (e_{prop}), and inclination (i_{prop}). The source number for each property is given in brackets. A machine readable version of this table is available on <https://zenodo.org/SOME-LINK>

[1] Minor Planet Center; 2020-12-08, <https://minorplanetcenter.net//iau/lists/JupiterTrojans.html>

[2] NEOWISE data v2.0, [Mainzer et al. \(2019\)](https://sbn.psi.edu/pds/resource/neowisediam.html), <https://sbn.psi.edu/pds/resource/neowisediam.html>

[3] Mira Brož ([Holt et al., 2020](#))

nr	prov. des.	H ^[1]	D [km] ^[2]	a_{prop} [au] ^[3]	e_{prop} ^[3]	i_{prop} [°] ^[3]
3548	1973 SO	9.85	63.885 ± 0.299	5.29758 ± 0.00065	0.04351 ± 0.00014	7.4150 ± 0.0012
5258	1989 AU1	10.33	53.275 ± 4.429	5.28801 ± 0.00115	0.05898 ± 0.00016	7.0285 ± 0.0018
8060	1973 SD1	10.95	37.873 ± 0.567	5.29164 ± 0.00054	0.05452 ± 0.00119	7.3082 ± 0.0006
9818	6591 P-L	11.07	28.076 ± 3.215	5.28832 ± 0.00114	0.04650 ± 0.00020	7.4624 ± 0.0092
13862	1999 XT160	11.6	24.835 ± 0.589	5.29245 ± 0.00012	0.04372 ± 0.00003	7.3313 ± 0.0004
18060	1999 XJ156	11.12	36.431 ± 3.966	5.29238 ± 0.00007	0.04448 ± 0.00003	7.4139 ± 0.0004
24380	2000 AA160	11.2	31.607 ± 0.266	5.29533 ± 0.00037	0.04358 ± 0.00006	7.3448 ± 0.0007
24420	2000 BU22	11.45	21.723 ± 1.211	5.30505 ± 0.00082	0.04881 ± 0.00022	7.2478 ± 0.0045
24426	2000 CR12	12.13	14.336 ± 1.007	5.30301 ± 0.00057	0.03817 ± 0.00041	7.3780 ± 0.0022
28958	2001 CQ42	12.18	21.577 ± 0.652	5.29703 ± 0.00102	0.03779 ± 0.00016	7.4208 ± 0.0011
39285	2001 BP75	12.49	17.602 ± 0.499	5.29535 ± 0.00054	0.04695 ± 0.00009	7.4102 ± 0.0008
39795	1997 SF28	12.42	18.342 ± 0.742	5.29306 ± 0.00012	0.05088 ± 0.00006	7.3939 ± 0.0003
43212	2000 AL113	12.2	19.212 ± 1.09	5.28911 ± 0.00082	0.04813 ± 0.00021	7.2695 ± 0.0059
43436	2000 YD42	12.12		5.29723 ± 0.00032	0.05201 ± 0.00007	7.1651 ± 0.0018
53469	2000 AX8	12.39	18.453 ± 0.354	5.30491 ± 0.00074	0.04462 ± 0.00015	7.4299 ± 0.0029
65150	2002 CA126	12.47		5.31311 ± 0.00198	0.04952 ± 0.00086	7.4866 ± 0.0392
65225	2002 EK44	12.36	16.654 ± 0.234	5.28639 ± 0.00032	0.04005 ± 0.00017	7.3903 ± 0.0031
88229	2001 BZ54	12.32		5.30633 ± 0.00041	0.05739 ± 0.00074	7.4842 ± 0.0022
89918	2002 ER33	12.8	12.373 ± 1.458	5.30353 ± 0.00068	0.03826 ± 0.00012	7.0953 ± 0.0015
101405	1998 VJ3	13.11		5.28464 ± 0.00060	0.04445 ± 0.00028	7.4773 ± 0.0027
111805	2002 CZ256	12.58		5.31320 ± 0.00192	0.04870 ± 0.00038	7.3476 ± 0.0488
127846	2003 FO111	12.47		5.28895 ± 0.00037	0.04116 ± 0.00009	7.5483 ± 0.0148
160661	1999 XD225	13.21	13.088 ± 0.703	5.28393 ± 0.00037	0.04216 ± 0.00018	7.5451 ± 0.0021
160856	2001 DU92	12.59	16.216 ± 0.54	5.29276 ± 0.00067	0.06018 ± 0.00168	7.3411 ± 0.0011
163135	2002 CT22	12.58	16.661 ± 0.735	5.28809 ± 0.00035	0.03962 ± 0.00011	7.4705 ± 0.0088
163189	2002 EU6	12.9	16.23 ± 0.781	5.30304 ± 0.00063	0.05173 ± 0.00027	7.3682 ± 0.0018
163216	2002 EN68	12.55	13.25 ± 0.801	5.29892 ± 0.00051	0.03974 ± 0.00008	7.2455 ± 0.0029
166211	2002 EP135	12.88	14.412 ± 1.052	5.29264 ± 0.00010	0.04550 ± 0.00004	7.4303 ± 0.0005
191088	2002 CP286	12.95		5.31470 ± 0.00274	0.05000 ± 0.00098	7.4788 ± 0.0463
191116	2002 ES84	13.1	13.023 ± 1.049	5.28790 ± 0.00054	0.06098 ± 0.00022	7.4879 ± 0.0018
192388	1996 RD29	12.91		5.29522 ± 0.00091	0.04449 ± 0.00016	7.3439 ± 0.0008
192929	2000 AT44	12.5	13.339 ± 0.482	5.29852 ± 0.00087	0.04532 ± 0.00028	7.3884 ± 0.0011

continuation on next page

nr	prov. des.	H ^[1]	D [km] ^[2]	a_{prop} [au] ^[3]	e_{prop} ^[3]	i_{prop} [°] ^[3]
195287	2002 EV79	13.32	12.908 ± 1.52	5.29829 ± 0.00154	0.05352 ± 0.00029	7.4974 ± 0.0016
195412	2002 GF39	12.45	19.051 ± 0.439	5.31429 ± 0.00208	0.04194 ± 0.00049	7.3980 ± 0.0437
200024	2007 OO7	12.8	13.808 ± 0.886	5.29731 ± 0.00107	0.04671 ± 0.00017	7.3943 ± 0.0007
200032	2007 PU43	12.89	17.945 ± 0.582	5.30250 ± 0.00101	0.04055 ± 0.00034	7.4355 ± 0.0008
210237	2007 RQ154	12.75	16.698 ± 0.713	5.31388 ± 0.00169	0.04575 ± 0.00091	7.4411 ± 0.0493
214376	2005 LF20	13.06		5.28327 ± 0.00027	0.04786 ± 0.00012	7.3828 ± 0.0012
219835	2002 CH82	13.29		5.29537 ± 0.00064	0.06259 ± 0.00012	7.2826 ± 0.0011
221786	2007 VA8	13.3		5.28067 ± 0.00024	0.04324 ± 0.00005	7.4014 ± 0.0011
222861	2002 EZ134	12.76	13.004 ± 0.896	5.28173 ± 0.00037	0.05655 ± 0.00008	7.2876 ± 0.0021
223251	2003 FB70	12.6	17.702 ± 0.529	5.28642 ± 0.00080	0.04997 ± 0.00010	7.3940 ± 0.0125
225214	2008 RM58	13.5	11.248 ± 0.758	5.29248 ± 0.00046	0.06430 ± 0.00023	7.3509 ± 0.0087
225222	2008 SP32	13.2	13.945 ± 0.652	5.30024 ± 0.00128	0.05227 ± 0.00017	7.4812 ± 0.0066
225227	2008 TO65	12.91	13.241 ± 0.835	5.29955 ± 0.00097	0.03513 ± 0.00014	7.4048 ± 0.0083
225359	1998 WJ24	13.5		5.29805 ± 0.00023	0.04484 ± 0.00006	7.2255 ± 0.0009
226067	2002 HQ14	12.9	14.325 ± 0.812	5.30220 ± 0.00078	0.04244 ± 0.00060	7.4595 ± 0.0012
228007	2007 RE27	13.52	11.085 ± 0.804	5.31435 ± 0.00191	0.04426 ± 0.00035	7.4952 ± 0.0391
228097	2008 SQ31	13.56	10.481 ± 0.819	5.29949 ± 0.00076	0.05814 ± 0.00013	7.4061 ± 0.0103
228098	2008 SM38	13.4		5.30782 ± 0.00042	0.04987 ± 0.00003	7.0712 ± 0.0066
228115	2008 TK76	13.41	12.813 ± 0.846	5.29906 ± 0.00117	0.04669 ± 0.00017	7.4664 ± 0.0012
228116	2008 TK82	13.48	12.81 ± 0.87	5.31022 ± 0.00218	0.03567 ± 0.00043	7.3475 ± 0.0426
229822	2008 TA112	13.38	13.975 ± 1.452	5.31046 ± 0.00229	0.04431 ± 0.00054	7.2730 ± 0.0355
233683	2008 RG113	13.79	10.171 ± 1.05	5.28352 ± 0.00075	0.04879 ± 0.00011	7.2041 ± 0.0018
237035	2008 SL91	13.37	11.96 ± 0.773	5.30419 ± 0.00044	0.04261 ± 0.00044	7.4308 ± 0.0013
243334	2008 TY109	13.4	12.583 ± 1.052	5.30130 ± 0.00060	0.04274 ± 0.00007	7.4938 ± 0.0020
246145	2007 PE9	13.21	12.093 ± 0.601	5.31229 ± 0.00160	0.04945 ± 0.00075	7.4333 ± 0.0487
247409	2002 CF79	12.94		5.30139 ± 0.00057	0.03952 ± 0.00016	7.3402 ± 0.0098
249247	2008 RV9	13.3	11.881 ± 0.689	5.32461 ± 0.00097	0.04832 ± 0.00051	7.5323 ± 0.0323
249256	2008 SH38	13.7	12.063 ± 1.353	5.29349 ± 0.00031	0.03868 ± 0.00008	7.3525 ± 0.0005
249481	2009 TE23	12.9	14.423 ± 0.534	5.28729 ± 0.00063	0.04362 ± 0.00011	7.3920 ± 0.0190
252683	2002 AE166	13		5.28721 ± 0.00094	0.04246 ± 0.00018	7.3334 ± 0.0081
252711	2002 CU152	13.2		5.28480 ± 0.00041	0.04693 ± 0.00011	7.2473 ± 0.0029
256553	2007 PT4	13.47	11.315 ± 1.321	5.28177 ± 0.00025	0.06126 ± 0.00007	7.2267 ± 0.0157
259316	2003 FJ38	13.9		5.29803 ± 0.00099	0.05018 ± 0.00018	7.4150 ± 0.0008
263822	2008 SO49	13.6	12.842 ± 1.575	5.28980 ± 0.00074	0.05301 ± 0.00029	7.2791 ± 0.0011
263829	2008 SL222	13.7		5.31818 ± 0.00090	0.04803 ± 0.00029	7.4725 ± 0.0113
263833	2008 TJ53	13.39		5.28277 ± 0.00066	0.04664 ± 0.00027	7.2566 ± 0.0015
264055	2009 SY5	13.9		5.30242 ± 0.00099	0.05524 ± 0.00019	7.5283 ± 0.0015
264071	2009 SW159	13.86	9.308 ± 0.786	5.30097 ± 0.00074	0.03994 ± 0.00020	7.3550 ± 0.0083
264101	2009 SN302	13.57		5.29128 ± 0.00011	0.04558 ± 0.00162	7.4393 ± 0.0010
264125	2009 TE35	12.87	14.906 ± 0.737	5.28883 ± 0.00059	0.05464 ± 0.00013	7.4805 ± 0.0067
264139	2009 UP78	13.4	14.172 ± 1.54	5.28924 ± 0.00115	0.05337 ± 0.00015	7.3813 ± 0.0017
264156	2009 WV5	13.2	14.642 ± 0.999	5.29478 ± 0.00033	0.06076 ± 0.00006	7.1825 ± 0.0007
264164	2010 AV106	13.4	11.165 ± 1.086	5.28071 ± 0.00028	0.06010 ± 0.00192	7.4667 ± 0.0310
264166	2010 AA123	13.02	16.478 ± 0.694	5.28619 ± 0.00071	0.04306 ± 0.00007	7.5722 ± 0.0141
266647	2008 SH229	13.56	10.752 ± 0.956	5.29690 ± 0.00049	0.05330 ± 0.00011	7.3024 ± 0.0024
266808	2009 SN355	13.6		5.29648 ± 0.00077	0.04771 ± 0.00008	7.3587 ± 0.0015
269327	2008 SC278	13.48	10.273 ± 0.943	5.29183 ± 0.00011	0.04481 ± 0.00127	7.6236 ± 0.0011
274675	2008 UZ7	13.3	11.657 ± 1.162	5.29177 ± 0.00029	0.05445 ± 0.00175	7.3320 ± 0.0005

continuation on next page

nr	prov. des.	H ^[1]	D [km] ^[2]	a_{prop} [au] ^[3]	e_{prop} ^[3]	i_{prop} [°] ^[3]
275116	2009 VD57	13.07	14.177 ± 0.73	5.28643 ± 0.00047	0.04272 ± 0.00010	7.4034 ± 0.0088
287577	2003 FE42	13.72		5.27778 ± 0.00006	0.05039 ± 0.00047	7.3046 ± 0.0010
295491	2008 RO20	14.07		5.29607 ± 0.00068	0.04676 ± 0.00012	7.5852 ± 0.0093
295500	2008 RQ45	14		5.28914 ± 0.00074	0.04246 ± 0.00044	7.3525 ± 0.0028
295503	2008 RE55	13.8		5.29274 ± 0.00007	0.04539 ± 0.00004	7.3813 ± 0.0006
295513	2008 RR82	14		5.28740 ± 0.00069	0.04094 ± 0.00015	7.4066 ± 0.0082
295520	2008 RP112	13.9	11.431 ± 1.236	5.27764 ± 0.00032	0.06030 ± 0.00010	7.5686 ± 0.0091
295625	2008 SM232	13.49		5.28435 ± 0.00022	0.03652 ± 0.00013	7.2870 ± 0.0011
295653	2008 TX4	13.2	11.381 ± 0.823	5.28964 ± 0.00058	0.05222 ± 0.00016	7.2854 ± 0.0012
295701	2008 TW174	13.28	15.821 ± 1.036	5.31444 ± 0.00302	0.04917 ± 0.00063	7.0421 ± 0.0288
296581	2009 RU8	13.69		5.28744 ± 0.00072	0.05135 ± 0.00013	7.4714 ± 0.0129
296604	2009 RT63	13.7		5.27814 ± 0.00025	0.04696 ± 0.00024	7.4235 ± 0.0015
306753	2000 YM25	13.58		5.29581 ± 0.00062	0.04419 ± 0.00012	7.3954 ± 0.0040
312461	2008 RK14	13.4	13.519 ± 1.195	5.29706 ± 0.00064	0.04519 ± 0.00008	7.4834 ± 0.0016
312620	2009 SA252	14.1		5.31502 ± 0.00190	0.05143 ± 0.00098	7.4341 ± 0.0386
312622	2009 SH313	13.5		5.29419 ± 0.00046	0.04565 ± 0.00007	7.4752 ± 0.0006
313024	2000 AV210	13.6	10.805 ± 0.599	5.28338 ± 0.00020	0.04545 ± 0.00004	7.4914 ± 0.0010
313323	2002 EJ152	13.66	10.133 ± 0.548	5.32028 ± 0.00016	0.05237 ± 0.00011	7.5301 ± 0.0050
315205	2007 QO15	13.6		5.31483 ± 0.00271	0.04237 ± 0.00018	7.4526 ± 0.0167
315915	2008 RB123	13.8		5.31239 ± 0.00195	0.04545 ± 0.00087	7.2461 ± 0.0689
315918	2008 RT126	14.04		5.28075 ± 0.00043	0.04211 ± 0.00007	7.2664 ± 0.0014
315925	2008 SE96	13.7		5.30192 ± 0.00135	0.06017 ± 0.00012	7.3595 ± 0.0074
315949	2008 TJ126	13.2		5.30950 ± 0.00252	0.03241 ± 0.00026	7.3091 ± 0.0470
315950	2008 TT127	13.76		5.29796 ± 0.00087	0.04443 ± 0.00014	7.3192 ± 0.0011
315954	2008 TJ176	13.76		5.31356 ± 0.00228	0.03449 ± 0.00043	7.3430 ± 0.0433
316130	2009 RA74	13.4	10.419 ± 0.714	5.28197 ± 0.00050	0.04700 ± 0.00008	7.3984 ± 0.0013
316157	2009 UT13	13.9		5.30583 ± 0.00019	0.03756 ± 0.00004	7.3313 ± 0.0016
316165	2009 VP110	13.2	13.8 ± 1.144	5.29951 ± 0.00104	0.06556 ± 0.00021	7.4262 ± 0.0103
316174	2009 WM250	13.4		5.29157 ± 0.00103	0.05899 ± 0.00075	7.2337 ± 0.0008
316267	2010 PW25	13.27		5.29297 ± 0.00008	0.05118 ± 0.00013	7.4478 ± 0.0006
316446	2010 UT53	13.8		5.31691 ± 0.00099	0.04948 ± 0.00017	7.4697 ± 0.0142
316484	2010 VM61	13.02		5.30616 ± 0.00016	0.04040 ± 0.00008	7.3078 ± 0.0023
316551	2010 XA84	13.8		5.29558 ± 0.00090	0.04624 ± 0.00010	7.3262 ± 0.0010
316552	2010 XF87	13.5		5.28917 ± 0.00154	0.05556 ± 0.00034	7.5163 ± 0.0060
321095	2008 SA277	13.9		5.28049 ± 0.00018	0.04834 ± 0.00006	7.2340 ± 0.0053
321113	2008 TQ131	13.8	11.395 ± 1.525	5.31471 ± 0.00253	0.04854 ± 0.00080	7.3964 ± 0.0491
321115	2008 TB142	13.7	10.609 ± 0.927	5.29233 ± 0.00041	0.05634 ± 0.00091	7.2441 ± 0.0011
321651	2010 BY9	13.5		5.29149 ± 0.00035	0.05112 ± 0.00032	7.4820 ± 0.0006
322540	2011 YR29	13.46		5.28473 ± 0.00024	0.04368 ± 0.00009	7.2906 ± 0.0015
325695	2009 UF23	13.29	11.631 ± 1.246	5.28760 ± 0.00030	0.03490 ± 0.00012	7.3411 ± 0.0035
328381	2008 RK41	14		5.29277 ± 0.00010	0.04957 ± 0.00013	7.4748 ± 0.0005
329008	2010 XZ64	14.1		5.30289 ± 0.00043	0.04933 ± 0.00034	7.3748 ± 0.0045
331050	2009 VH107	13.4	13.071 ± 1.317	5.31320 ± 0.00196	0.05211 ± 0.00144	7.3619 ± 0.0438
339562	2005 JF162	13.67		5.27697 ± 0.00021	0.04141 ± 0.00206	7.8027 ± 0.0008
344629	2003 JL18	13.7		5.29654 ± 0.00082	0.03912 ± 0.00012	7.3092 ± 0.0045
347148	2010 WY	13.03		5.29512 ± 0.00021	0.05222 ± 0.00004	7.3093 ± 0.0005
349919	2009 SZ166	14.02		5.31938 ± 0.00039	0.04372 ± 0.00006	7.3587 ± 0.0015
350051	2010 PH25	13.4		5.29811 ± 0.00053	0.05914 ± 0.00013	7.3911 ± 0.0064
350053	2010 PE49	13.9		5.29406 ± 0.00057	0.04311 ± 0.00010	7.3709 ± 0.0006
350825	2002 ER38	13.94		5.31152 ± 0.00183	0.04263 ± 0.00034	7.3857 ± 0.0281
352662	2008 RM14	13.71	10.434 ± 1.344	5.30011 ± 0.00108	0.05428 ± 0.00011	7.3620 ± 0.0016
352668	2008 RQ72	13.43		5.29113 ± 0.00075	0.05216 ± 0.00090	7.2939 ± 0.0007
352793	2008 UF189	14.01		5.29618 ± 0.00049	0.03654 ± 0.00012	7.3371 ± 0.0011

continuation on next page

nr	prov. des.	H ^[1]	D [km] ^[2]	a_{prop} [au] ^[3]	e_{prop} ^[3]	i_{prop} [°] ^[3]
353180	2009 RG14	13.8		5.29676 ± 0.00068	0.04648 ± 0.00014	7.2963 ± 0.0071
353188	2009 RR68	13.8		5.31651 ± 0.00216	0.04966 ± 0.00059	7.3922 ± 0.0313
353193	2009 SH58	14		5.28823 ± 0.00141	0.06085 ± 0.00058	7.4283 ± 0.0020
353209	2009 SC354	13.7		5.28398 ± 0.00020	0.03485 ± 0.00009	7.1710 ± 0.0011
353346	2010 VV78	14		5.29266 ± 0.00005	0.04259 ± 0.00002	7.2241 ± 0.0005
353350	2010 VA116	13.81		5.29909 ± 0.00041	0.04136 ± 0.00009	7.3588 ± 0.0012
353351	2010 VO138	13.6		5.27589 ± 0.00014	0.05045 ± 0.00334	7.2139 ± 0.0027
353356	2010 VZ214	14.28		5.27930 ± 0.00017	0.04828 ± 0.00009	7.5331 ± 0.0012
353740	2011 YB18	13.8		5.30786 ± 0.00033	0.04839 ± 0.00014	7.4186 ± 0.0019
353743	2011 YN40	13.4		5.28479 ± 0.00042	0.04311 ± 0.00008	7.2671 ± 0.0012
353744	2011 YL45	13.7		5.29042 ± 0.00030	0.04851 ± 0.00008	7.5597 ± 0.0012
355756	2008 QL37	14	8.864 ± 0.965	5.29335 ± 0.00008	0.05546 ± 0.00115	7.5500 ± 0.0010
355760	2008 RQ10	13.8	10.436 ± 1.217	5.27905 ± 0.00023	0.06265 ± 0.00260	7.2633 ± 0.0286
355765	2008 RK37	13.8	10.896 ± 1.228	5.28833 ± 0.00061	0.04196 ± 0.00037	7.2167 ± 0.0189
355809	2008 SK277	14		5.29128 ± 0.00010	0.04742 ± 0.00012	7.6100 ± 0.0010
355814	2008 TU37	14.1	9.472 ± 1.234	5.30388 ± 0.00088	0.04402 ± 0.00018	7.2709 ± 0.0012
355820	2008 TY96	13.9		5.28068 ± 0.00026	0.04945 ± 0.00006	7.5335 ± 0.0035
355849	2008 UM109	13.7		5.30381 ± 0.00045	0.04619 ± 0.00067	7.4654 ± 0.0016
356211	2009 RB63	14		5.31729 ± 0.00061	0.04073 ± 0.00014	7.2387 ± 0.0036
356222	2009 SF194	14		5.28878 ± 0.00048	0.04667 ± 0.00029	7.1184 ± 0.0025
356240	2009 SB354	13.9		5.28760 ± 0.00093	0.05710 ± 0.00040	7.4233 ± 0.0024
356248	2009 UO12	14.29		5.31471 ± 0.00226	0.04748 ± 0.00049	7.1598 ± 0.0443
356257	2009 UL140	13.5	10.569 ± 0.716	5.30676 ± 0.00090	0.05552 ± 0.00035	7.3423 ± 0.0096
356259	2009 UV148	13.8	10.806 ± 1.499	5.29962 ± 0.00108	0.04990 ± 0.00017	7.4413 ± 0.0119
356270	2009 WJ107	13.8		5.28651 ± 0.00048	0.04214 ± 0.00010	7.2332 ± 0.0066
356284	2010 CH242	14	12.435 ± 1.383	5.31080 ± 0.00209	0.04047 ± 0.00055	7.5234 ± 0.0418
356426	2010 VB122	14.3		5.28686 ± 0.00045	0.04039 ± 0.00010	7.3568 ± 0.0034
356441	2010 XX7	14.04		5.26719 ± 0.00038	0.04188 ± 0.00011	7.8568 ± 0.0021
356449	2010 XO79	13.9		5.28290 ± 0.00046	0.04878 ± 0.00015	7.2260 ± 0.0019
356902	2011 YF56	14.1		5.28822 ± 0.00104	0.04660 ± 0.00022	7.4036 ± 0.0073
356905	2011 YC75	14		5.28747 ± 0.00152	0.06048 ± 0.00026	7.3071 ± 0.0031
356913	2012 BQ50	13.8		5.29908 ± 0.00114	0.05636 ± 0.00011	7.4266 ± 0.0018
359345	2009 SE198	14.18		5.30233 ± 0.00179	0.04102 ± 0.00034	7.6295 ± 0.0081
359360	2009 US28	14.3	9.742 ± 1.077	5.30179 ± 0.00100	0.05517 ± 0.00014	7.4536 ± 0.0017
359361	2009 US55	14.1	10.084 ± 1.028	5.28199 ± 0.00053	0.05477 ± 0.00012	7.4286 ± 0.0024
359368	2009 WC57	13.7	12.764 ± 0.907	5.28701 ± 0.00053	0.04424 ± 0.00014	7.4095 ± 0.0062
359594	2010 VF86	13.9		5.28178 ± 0.00093	0.05059 ± 0.00005	7.4159 ± 0.0010
359943	2011 YG75	13.9		5.29676 ± 0.00105	0.04762 ± 0.00018	7.3808 ± 0.0010
360031	2013 AA30	13.4		5.28629 ± 0.00052	0.04119 ± 0.00014	7.2746 ± 0.0125
360072	2013 AJ131	13.59		5.28560 ± 0.00074	0.05403 ± 0.00019	7.4961 ± 0.0051
360076	2013 AE132	14.1		5.31595 ± 0.00174	0.04672 ± 0.00122	7.3339 ± 0.0497
360079	2013 BM1	13.96		5.28989 ± 0.00116	0.05861 ± 0.00027	7.2547 ± 0.0010
361999	2008 TV96	13.8	9.092 ± 1.079	5.29518 ± 0.00055	0.05280 ± 0.00007	7.4544 ± 0.0009
365037	2008 SQ261	13.8		5.30437 ± 0.00060	0.04333 ± 0.00025	7.4032 ± 0.0053
366254	2012 YY2	14		5.29325 ± 0.00017	0.04472 ± 0.00003	7.1988 ± 0.0003
366317	2013 CV197	14.3		5.28734 ± 0.00049	0.06332 ± 0.00058	7.3557 ± 0.0041
386967	2011 YS34	14.1		5.30048 ± 0.00092	0.05866 ± 0.00016	7.4433 ± 0.0017
387390	2013 AG133	13.85		5.30063 ± 0.00085	0.05499 ± 0.00014	7.5039 ± 0.0021
388891	2008 RW128	14.1		5.28979 ± 0.00039	0.04778 ± 0.00008	7.5998 ± 0.0014
389317	2009 ST140	13.81		5.29662 ± 0.00034	0.04968 ± 0.00016	7.3088 ± 0.0016
389318	2009 SV169	13.69		5.30732 ± 0.00050	0.05871 ± 0.00020	7.5124 ± 0.0050
389327	2009 SB248	14.1		5.29868 ± 0.00081	0.05169 ± 0.00010	7.5249 ± 0.0080

continuation on next page

nr	prov. des.	H ^[1]	D [km] ^[2]	a_{prop} [au] ^[3]	e_{prop} ^[3]	i_{prop} [°] ^[3]
389332	2009 SF283	14		5.31827 ± 0.00031	0.03955 ± 0.00009	7.5303 ± 0.0012
389560	2010 UN93	14.41		5.27717 ± 0.00020	0.04674 ± 0.00023	7.2522 ± 0.0008
389823	2011 YP24	13.6		5.29054 ± 0.00099	0.05515 ± 0.00059	7.3108 ± 0.0011
389824	2011 YH75	13.8		5.28569 ± 0.00092	0.04548 ± 0.00011	7.3626 ± 0.0027
390322	2013 BA1	13.66		5.29003 ± 0.00110	0.05025 ± 0.00038	7.4194 ± 0.0011
390344	2013 CP95	14		5.27738 ± 0.00014	0.05332 ± 0.00288	7.3953 ± 0.0072
390347	2013 CU111	13.9		5.29198 ± 0.00010	0.04749 ± 0.00094	7.5701 ± 0.0007
390349	2013 CG140	13.8		5.29426 ± 0.00048	0.04458 ± 0.00010	7.5158 ± 0.0008
390352	2013 CY173	14.1		5.29654 ± 0.00064	0.05671 ± 0.00017	7.2346 ± 0.0008
390358	2013 CC207	14.09		5.31568 ± 0.00252	0.05347 ± 0.00038	7.2911 ± 0.0471
390362	2013 CQ217	14		5.28810 ± 0.00082	0.04783 ± 0.00010	7.1941 ± 0.0208
391792	2008 RE70	13.8		5.29958 ± 0.00100	0.04749 ± 0.00012	7.4788 ± 0.0016
392206	2009 SR301	14.1		5.30218 ± 0.00099	0.04990 ± 0.00011	7.5211 ± 0.0021
392227	2009 VK8	14.3		5.28967 ± 0.00049	0.04059 ± 0.00067	7.1532 ± 0.0057
392239	2009 WP12	14.1		5.30136 ± 0.00221	0.05854 ± 0.00059	7.3537 ± 0.0056
392309	2010 CO226	13.8		5.29454 ± 0.00070	0.04672 ± 0.00009	7.4336 ± 0.0007
392460	2010 XY9	14.2		5.28852 ± 0.00082	0.05463 ± 0.00016	7.1938 ± 0.0013
392461	2010 XT65	13.8		5.30296 ± 0.00075	0.04292 ± 0.00081	7.3692 ± 0.0054
392462	2010 XB77	14		5.28677 ± 0.00038	0.04370 ± 0.00023	7.4404 ± 0.0160
392703	2011 YD71	13.99		5.30436 ± 0.00020	0.04431 ± 0.00023	7.5656 ± 0.0026
393144	2013 BT60	13.9		5.27854 ± 0.00022	0.03530 ± 0.00003	7.2506 ± 0.0006
396140	2013 DU5	14.3		5.29170 ± 0.00114	0.05931 ± 0.00163	7.0662 ± 0.0066
396159	2013 EA41	14.2		5.28863 ± 0.00059	0.06009 ± 0.00013	7.2481 ± 0.0016
398616	2011 YB3	13.76		5.31244 ± 0.00179	0.04938 ± 0.00096	7.3522 ± 0.0659
398800	2013 BZ	13.6		5.28664 ± 0.00044	0.04249 ± 0.00017	7.3071 ± 0.0077
412432	2014 EG31	13.8		5.31418 ± 0.00148	0.05128 ± 0.00075	7.3086 ± 0.0429
426992	2014 DQ67	13.9		5.27808 ± 0.00014	0.04964 ± 0.00024	7.3384 ± 0.0015
429083	2009 RP8	13.88		5.29211 ± 0.00034	0.05797 ± 0.00104	7.2907 ± 0.0012
429974	2013 BM26	14.13		5.30657 ± 0.00035	0.04039 ± 0.00004	7.4304 ± 0.0017
432264	2009 SZ27	13.8		5.31168 ± 0.00248	0.04355 ± 0.00041	7.4915 ± 0.0293
432629	2010 VC94	14		5.29806 ± 0.00158	0.04914 ± 0.00017	7.3217 ± 0.0014
433275	2013 AT93	13.4		5.27857 ± 0.00038	0.05520 ± 0.00288	7.5284 ± 0.0026
433277	2013 AT108	14.26		5.31241 ± 0.00190	0.04306 ± 0.00070	7.5192 ± 0.0491
433287	2013 BU44	14.34		5.31429 ± 0.00217	0.04826 ± 0.00062	7.4642 ± 0.0360
433295	2013 CV209	14.1		5.28100 ± 0.00017	0.04283 ± 0.00011	7.8006 ± 0.0010
433297	2013 DE13	14.1		5.28819 ± 0.00101	0.04512 ± 0.00014	7.3759 ± 0.0111
433671	2014 DF32	14.1		5.29003 ± 0.00055	0.05379 ± 0.00011	7.3922 ± 0.0019
433674	2014 DH124	14.3		5.30483 ± 0.00051	0.03978 ± 0.00008	7.6044 ± 0.0049
435573	2008 RA82	14.3		5.29164 ± 0.00006	0.03941 ± 0.00005	7.5508 ± 0.0011
435632	2008 SB137	14		5.29411 ± 0.00014	0.05613 ± 0.00038	7.5447 ± 0.0005
436061	2009 RR64	14.4		5.29293 ± 0.00017	0.05436 ± 0.00121	7.5227 ± 0.0011
436072	2009 SA98	13.9		5.30690 ± 0.00114	0.05462 ± 0.00032	7.5325 ± 0.0033
436107	2009 SR319	14.2		5.28011 ± 0.00042	0.04347 ± 0.00019	7.7064 ± 0.0010
436124	2009 TZ28	14.3		5.29636 ± 0.00062	0.04163 ± 0.00018	7.4197 ± 0.0042
436409	2010 XW81	14.1		5.29320 ± 0.00027	0.04243 ± 0.00004	7.6353 ± 0.0007
436760	2012 BW68	13.9		5.31593 ± 0.00150	0.04952 ± 0.00068	7.1467 ± 0.0422
437310	2013 CN206	14.4		5.28275 ± 0.00013	0.03778 ± 0.00007	7.3191 ± 0.0030
437311	2013 CF217	14		5.29774 ± 0.00036	0.04393 ± 0.00009	7.3502 ± 0.0081
437720	2014 DB110	14		5.28538 ± 0.00062	0.06135 ± 0.00038	7.4157 ± 0.0034
466239	2013 BU16	14.3		5.30609 ± 0.00030	0.04598 ± 0.00005	7.4806 ± 0.0021
467635	2008 RV54	14.2		5.29488 ± 0.00022	0.05657 ± 0.00002	7.2476 ± 0.0004
468015	2013 BB54	14.17		5.30783 ± 0.00056	0.04382 ± 0.00004	7.4237 ± 0.0057
469163	2015 HD140	14.5		5.27488 ± 0.00014	0.03784 ± 0.00226	7.3685 ± 0.0006
489949	2008 RS112	14.4		5.29748 ± 0.00073	0.05043 ± 0.00014	7.3571 ± 0.0119

continuation on next page

nr	prov. des.	H ^[1]	D [km] ^[2]	a_{prop} [au] ^[3]	e_{prop} ^[3]	i_{prop} [°] ^[3]
490809	2010 VE115	14.3		5.28136 ± 0.00044	0.04804 ± 0.00012	7.2990 ± 0.0013
490817	2010 VF142	14.1		5.30254 ± 0.00071	0.04120 ± 0.00012	7.6373 ± 0.0027
490820	2010 VA148	14.6		5.29666 ± 0.00072	0.04077 ± 0.00013	7.3406 ± 0.0096
490839	2010 WD33	14.4		5.29024 ± 0.00012	0.04269 ± 0.00008	7.5648 ± 0.0021
491834	2013 AQ39	14.2		5.28135 ± 0.00044	0.04558 ± 0.00012	7.4938 ± 0.0019
491937	2013 CJ112	13.8		5.29918 ± 0.00058	0.04790 ± 0.00015	7.3347 ± 0.0009
493531	2015 FF112	13.8		5.29339 ± 0.00025	0.04621 ± 0.00005	7.3987 ± 0.0009
493534	2015 FU206	14.4		5.30315 ± 0.00108	0.04944 ± 0.00058	7.4456 ± 0.0016
495194	2013 BH	14.1		5.29243 ± 0.00020	0.04804 ± 0.00003	7.1808 ± 0.0004
496031	2008 SR274	13.9		5.29794 ± 0.00060	0.05049 ± 0.00011	7.3290 ± 0.0113
496300	2013 CV194	14.4		5.28224 ± 0.00032	0.04208 ± 0.00010	7.3580 ± 0.0027
507354	2011 UQ402	14.47		5.30687 ± 0.00034	0.05115 ± 0.00015	7.2940 ± 0.0032
507370	2011 YF75	14.2		5.29222 ± 0.00029	0.04961 ± 0.00009	7.1441 ± 0.0008
510519	2012 BB155	14.1		5.31695 ± 0.00119	0.04861 ± 0.00042	7.1741 ± 0.0400
542169	2013 AD8	13.57		5.30997 ± 0.00214	0.04463 ± 0.00050	7.3777 ± 0.0201
542262	2013 BL	13.7		5.28851 ± 0.00085	0.05481 ± 0.00031	7.2794 ± 0.0011
542275	2013 BY16	13.88		5.30581 ± 0.00036	0.04280 ± 0.00004	7.3603 ± 0.0031
542323	2013 CR12	14.2		5.31364 ± 0.00221	0.05294 ± 0.00082	7.3147 ± 0.0535
542399	2013 CH95	13.9		5.28234 ± 0.00036	0.04884 ± 0.00021	7.4420 ± 0.0007
546419	2010 VJ119	14.3		5.29841 ± 0.00059	0.04121 ± 0.00008	7.1403 ± 0.0062
546454	2010 VD159	14.2		5.29055 ± 0.00013	0.03987 ± 0.00013	7.3569 ± 0.0018
546460	2010 VF166	14.4		5.28463 ± 0.00034	0.05069 ± 0.00021	7.3203 ± 0.0068
546752	2010 XO67	14.2		5.28369 ± 0.00026	0.04545 ± 0.00022	7.2955 ± 0.0014
	2001 DD120	14.6		5.30468 ± 0.00042	0.04027 ± 0.00007	7.3710 ± 0.0016
	2002 EF171	14.3		5.28473 ± 0.00042	0.05087 ± 0.00019	7.3110 ± 0.0208
	2002 EN157	14.3		5.29465 ± 0.00013	0.05854 ± 0.00005	7.3953 ± 0.0005
	2002 FA42	14.1		5.30186 ± 0.00113	0.03801 ± 0.00025	7.4180 ± 0.0021
	2002 FJ19	14.5		5.30476 ± 0.00052	0.03945 ± 0.00008	7.3969 ± 0.0026
	2002 GH197	14.2		5.31591 ± 0.00210	0.04975 ± 0.00048	7.3294 ± 0.0204
	2003 DU22	14.4		5.30681 ± 0.00016	0.04334 ± 0.00003	7.3131 ± 0.0012
	2003 GO64	14.3		5.27865 ± 0.00009	0.03853 ± 0.00004	7.3525 ± 0.0006
	2004 GK85	13.7		5.30908 ± 0.00145	0.03367 ± 0.00034	7.3711 ± 0.0189
	2005 DK4	14.4		5.29447 ± 0.00040	0.04522 ± 0.00006	7.3736 ± 0.0008
	2007 RE166	14.5		5.31145 ± 0.00272	0.04864 ± 0.00079	7.3026 ± 0.0660
	2008 QK42	14.4		5.29834 ± 0.00030	0.04608 ± 0.00005	7.4727 ± 0.0016
	2008 RC150	14.2		5.31403 ± 0.00320	0.04545 ± 0.00060	7.3809 ± 0.0448
	2008 RG65	14.2		5.30187 ± 0.00037	0.05455 ± 0.00017	7.5069 ± 0.0026
	2008 RK127	14.1		5.29491 ± 0.00071	0.05326 ± 0.00010	7.4462 ± 0.0006
	2008 RR161	13.9		5.31944 ± 0.00048	0.04781 ± 0.00014	7.4598 ± 0.0026
	2008 RS149	14.2		5.30661 ± 0.00035	0.03531 ± 0.00010	7.3202 ± 0.0007
	2008 SH232	14.1		5.29076 ± 0.00016	0.04943 ± 0.00005	7.5983 ± 0.0009
	2008 SP275	14.4		5.31820 ± 0.00049	0.04420 ± 0.00015	7.5274 ± 0.0033
	2008 SU275	14.4		5.27953 ± 0.00022	0.04626 ± 0.00004	7.2280 ± 0.0011
	2008 SW73	14.1		5.28853 ± 0.00049	0.04498 ± 0.00011	7.3335 ± 0.0113
	2008 TF194	14.2		5.27891 ± 0.00038	0.04682 ± 0.00009	7.2062 ± 0.0014
	2008 TH97	14.4		5.29052 ± 0.00090	0.05304 ± 0.00020	7.4797 ± 0.0009
	2008 UQ400	14.3		5.29320 ± 0.00010	0.04769 ± 0.00003	7.2687 ± 0.0003
	2008 UW376	13.6		5.27183 ± 0.00028	0.04282 ± 0.00007	7.6491 ± 0.0032
	2008 UY128	13.8		5.29182 ± 0.00018	0.04855 ± 0.00106	7.4447 ± 0.0006
	2009 RG57	14.3		5.28692 ± 0.00059	0.05348 ± 0.00017	7.4748 ± 0.0071
	2009 RM64	14.7		5.30844 ± 0.00085	0.04780 ± 0.00009	7.2830 ± 0.0026
	2009 SB326	13.6		5.28234 ± 0.00039	0.05007 ± 0.00005	7.2500 ± 0.0012
	2009 SF148	14.3		5.27451 ± 0.00016	0.05702 ± 0.00004	7.5491 ± 0.0010

continuation on next page

nr	prov. des.	H ^[1]	D [km] ^[2]	a_{prop} [au] ^[3]	e_{prop} ^[3]	i_{prop} [°] ^[3]
2009	SF391	14.4		5.28771 ± 0.00116	0.04943 ± 0.00014	7.4115 ± 0.0040
2009	SG355	14.7		5.28988 ± 0.00103	0.05970 ± 0.00035	7.1440 ± 0.0009
2009	SJ389	14.1		5.28780 ± 0.00052	0.05348 ± 0.00016	7.2953 ± 0.0018
2009	SL48	14.3		5.29257 ± 0.00014	0.05293 ± 0.00087	7.4199 ± 0.0008
2009	SM188	14.3		5.28991 ± 0.00081	0.04962 ± 0.00019	7.5482 ± 0.0022
2009	SS301	14.4		5.30166 ± 0.00102	0.03807 ± 0.00011	7.6573 ± 0.0017
2009	SU355	14.4		5.28688 ± 0.00119	0.04673 ± 0.00010	7.5896 ± 0.0152
2009	SX354	14.3		5.31025 ± 0.00200	0.04025 ± 0.00066	7.4104 ± 0.0409
2009	SX391	14.6		5.28473 ± 0.00044	0.05196 ± 0.00016	7.3298 ± 0.0056
2009	SY373	13.6		5.31678 ± 0.00281	0.04902 ± 0.00028	7.3629 ± 0.0137
2009	TR53	13.7		5.31481 ± 0.00163	0.05976 ± 0.00101	7.5387 ± 0.0689
2009	UD168	14.5		5.28525 ± 0.00022	0.04205 ± 0.00017	7.3752 ± 0.0014
2009	UE159	14		5.28742 ± 0.00078	0.04558 ± 0.00021	7.3363 ± 0.0100
2009	UG170	14.3		5.30536 ± 0.00028	0.04409 ± 0.00013	7.3725 ± 0.0023
2009	UG57	14.3		5.27916 ± 0.00044	0.03975 ± 0.00004	7.2532 ± 0.0009
2009	VF54	14.6		5.29727 ± 0.00022	0.06547 ± 0.00004	7.3167 ± 0.0005
2009	WA142	14.6		5.30374 ± 0.00126	0.05554 ± 0.00057	7.4370 ± 0.0081
2009	WJ160	14.6		5.28212 ± 0.00008	0.03844 ± 0.00006	7.3186 ± 0.0011
2009	WO137	14.3		5.30489 ± 0.00090	0.04793 ± 0.00017	7.3540 ± 0.0023
2010	TW192	14.4		5.28852 ± 0.00129	0.05533 ± 0.00014	7.4029 ± 0.0016
2010	VF136	14.8		5.28704 ± 0.00033	0.04538 ± 0.00020	7.7117 ± 0.0067
2010	VS244	14.5		5.31323 ± 0.00256	0.04733 ± 0.00068	7.6120 ± 0.0400
2010	VZ224	14.2		5.28210 ± 0.00023	0.04333 ± 0.00010	7.5051 ± 0.0040
2010	WZ18	14.6		5.30468 ± 0.00034	0.04693 ± 0.00106	7.6465 ± 0.0021
2010	XD106	14.6		5.28778 ± 0.00064	0.05005 ± 0.00025	7.6303 ± 0.0046
2010	XU106	14.7		5.28342 ± 0.00047	0.04492 ± 0.00009	7.2284 ± 0.0009
2011	WG69	14		5.30854 ± 0.00036	0.05201 ± 0.00006	7.4741 ± 0.0053
2011	XY1	14.3		5.28374 ± 0.00035	0.05212 ± 0.00021	7.4192 ± 0.0042
2011	YM90	14.9		5.28670 ± 0.00127	0.06035 ± 0.00043	7.3066 ± 0.0031
2012	BD155	14.2		5.29424 ± 0.00037	0.03578 ± 0.00007	7.3295 ± 0.0010
2012	BU107	14.8		5.30454 ± 0.00041	0.03862 ± 0.00017	6.9884 ± 0.0027
2012	BU172	14.6		5.28615 ± 0.00070	0.04572 ± 0.00011	7.4598 ± 0.0067
2012	CT57	14.9		5.28805 ± 0.00088	0.03928 ± 0.00061	7.1233 ± 0.0058
2012	YS9	14.7		5.31481 ± 0.00211	0.04758 ± 0.00126	7.2766 ± 0.0310
2013	AJ133	14.2		5.30577 ± 0.00014	0.04198 ± 0.00005	7.2517 ± 0.0017
2013	AN129	13.8		5.29564 ± 0.00094	0.04982 ± 0.00017	7.4682 ± 0.0034
2013	AS64	14.3		5.28135 ± 0.00042	0.04573 ± 0.00007	7.2800 ± 0.0026
2013	AU35	13.8		5.28124 ± 0.00037	0.04027 ± 0.00006	7.5409 ± 0.0009
2013	AV135	13.8		5.31461 ± 0.00238	0.04957 ± 0.00068	7.4961 ± 0.0166
2013	BB17	14.5		5.28462 ± 0.00083	0.05590 ± 0.00046	7.2268 ± 0.0089
2013	BD	14.3		5.30519 ± 0.00019	0.04708 ± 0.00023	7.4620 ± 0.0021
2013	BD17	14.3		5.31308 ± 0.00327	0.03312 ± 0.00031	7.2749 ± 0.0234
2013	BE	14.6		5.27946 ± 0.00036	0.06045 ± 0.00412	7.5400 ± 0.0336
2013	BF	14.8		5.27734 ± 0.00018	0.06126 ± 0.00018	7.5134 ± 0.0041
2013	BH31	14.1		5.28954 ± 0.00044	0.04440 ± 0.00018	7.4044 ± 0.0038
2013	BJ11	14.2		5.29671 ± 0.00056	0.04226 ± 0.00012	7.3170 ± 0.0010
2013	BO82	14.7		5.28089 ± 0.00018	0.04770 ± 0.00006	7.1978 ± 0.0015
2013	BP34	14.1		5.29500 ± 0.00018	0.05958 ± 0.00003	7.3897 ± 0.0006
2013	BR1	14.6		5.29265 ± 0.00011	0.03961 ± 0.00002	7.3226 ± 0.0009
2013	BR7	14.2		5.30335 ± 0.00042	0.04797 ± 0.00024	7.5073 ± 0.0027
2013	BS38	14.1		5.28510 ± 0.00076	0.06048 ± 0.00014	7.3364 ± 0.0067
2013	BV16	14.1		5.29393 ± 0.00020	0.04694 ± 0.00003	7.4546 ± 0.0003

continuation on next page

nr	prov. des.	H ^[1]	D [km] ^[2]	a_{prop} [au] ^[3]	e_{prop} ^[3]	i_{prop} [°] ^[3]
	2013 BV41	14.4		5.30819 ± 0.00052	0.06525 ± 0.00028	7.4349 ± 0.0062
	2013 BZ15	14.6		5.31549 ± 0.00176	0.03840 ± 0.00051	7.3675 ± 0.0240
	2013 CC160	14.4		5.31225 ± 0.00259	0.03949 ± 0.00042	7.3507 ± 0.0322
	2013 CF200	14.4		5.28209 ± 0.00031	0.05150 ± 0.00007	7.2651 ± 0.0014
	2013 CH204	14.2		5.28950 ± 0.00030	0.03898 ± 0.00025	7.1040 ± 0.0095
	2013 CM101	14.2		5.29647 ± 0.00063	0.04090 ± 0.00010	7.3218 ± 0.0010
	2013 CM11	14.3		5.29468 ± 0.00015	0.06154 ± 0.00094	7.5909 ± 0.0007
	2013 CM170	14.1		5.30052 ± 0.00044	0.03613 ± 0.00017	7.3288 ± 0.0060
	2013 CM223	15.1		5.30406 ± 0.00059	0.05235 ± 0.00042	7.4547 ± 0.0014
	2013 CN157	14.4		5.28020 ± 0.00049	0.04938 ± 0.00017	7.5830 ± 0.0016
	2013 CO93	14.4		5.29310 ± 0.00008	0.05221 ± 0.00005	7.3486 ± 0.0007
	2013 CR223	14.4		5.27789 ± 0.00015	0.04084 ± 0.00005	7.2760 ± 0.0006
	2013 CS194	14.3		5.27927 ± 0.00034	0.05332 ± 0.00015	7.3158 ± 0.0083
	2013 EL154	14.8		5.28408 ± 0.00054	0.04349 ± 0.00035	7.6092 ± 0.0031
	2013 EM154	14.1		5.30736 ± 0.00029	0.05066 ± 0.00005	7.4626 ± 0.0020
	2014 DM49	14.2		5.28727 ± 0.00066	0.04609 ± 0.00022	7.2591 ± 0.0112
	2014 DX143	14.7		5.30650 ± 0.00020	0.04372 ± 0.00012	7.6318 ± 0.0003
	2014 EG188	14.3		5.29268 ± 0.00015	0.04449 ± 0.00002	7.2062 ± 0.0005
	2014 EG68	14.1		5.27838 ± 0.00020	0.06209 ± 0.00309	7.2843 ± 0.0347
	2014 EK55	14.6		5.29908 ± 0.00106	0.05083 ± 0.00014	7.1927 ± 0.0071
	2014 EL155	14.1		5.28982 ± 0.00079	0.04643 ± 0.00045	7.2772 ± 0.0021
	2014 EM36	13.7		5.29154 ± 0.00020	0.04560 ± 0.00014	7.3784 ± 0.0005
	2014 EO56	14.7		5.31810 ± 0.00047	0.04720 ± 0.00015	7.1782 ± 0.0048
	2014 ES95	14.4		5.29502 ± 0.00060	0.04928 ± 0.00016	7.6065 ± 0.0054
	2014 ET118	14.9		5.28428 ± 0.00026	0.04316 ± 0.00007	7.4103 ± 0.0015
	2014 EV177	14.9		5.30861 ± 0.00035	0.05480 ± 0.00008	7.5591 ± 0.0024
	2014 EV198	14.4		5.28998 ± 0.00031	0.03772 ± 0.00011	7.0962 ± 0.0064
	2014 EV65	14.5		5.28611 ± 0.00018	0.05235 ± 0.00010	7.1992 ± 0.0234
	2014 EW31	13.9		5.28190 ± 0.00027	0.04854 ± 0.00010	7.2329 ± 0.0017
	2014 EX69	14.1		5.28533 ± 0.00028	0.05137 ± 0.00004	7.3139 ± 0.0042
	2014 EZ194	14.4		5.28941 ± 0.00104	0.05286 ± 0.00058	7.2121 ± 0.0013
	2014 EZ84	14.5		5.28838 ± 0.00059	0.04797 ± 0.00022	7.3654 ± 0.0100
	2014 FD72	14.6		5.30554 ± 0.00059	0.04434 ± 0.00020	7.3119 ± 0.0017
	2014 FG5	14.6		5.29643 ± 0.00054	0.05283 ± 0.00016	7.3145 ± 0.0030
	2014 FT43	14.5		5.30899 ± 0.00107	0.04689 ± 0.00024	7.3105 ± 0.0286
	2014 GL9	14.2		5.28302 ± 0.00023	0.04723 ± 0.00011	7.3426 ± 0.0013
	2014 GM9	13.6		5.32418 ± 0.00232	0.04061 ± 0.00044	7.4104 ± 0.0117
	2014 GN10	13.9		5.28296 ± 0.00060	0.04155 ± 0.00018	7.1739 ± 0.0014
	2015 DT225	14		5.30021 ± 0.00120	0.05943 ± 0.00026	7.4643 ± 0.0117
	2015 FF354	14.2		5.28313 ± 0.00031	0.04028 ± 0.00011	7.3431 ± 0.0020
	2015 FJ139	14.3		5.28480 ± 0.00041	0.04974 ± 0.00024	7.5923 ± 0.0052
	2015 FJ74	14.1		5.30446 ± 0.00041	0.04539 ± 0.00022	7.2931 ± 0.0034
	2015 FQ211	14.4		5.28382 ± 0.00051	0.04879 ± 0.00056	7.2638 ± 0.0026
	2015 FQ305	14.4		5.31609 ± 0.00206	0.04965 ± 0.00059	7.4760 ± 0.0415
	2015 FQ357	14.2		5.29301 ± 0.00011	0.04931 ± 0.00002	7.2904 ± 0.0004
	2015 FR388	13.9		5.30710 ± 0.00022	0.04775 ± 0.00003	7.3857 ± 0.0019
	2015 FT170	14.3		5.31481 ± 0.00161	0.04912 ± 0.00093	7.1663 ± 0.0734
	2015 HL89	14.1		5.27779 ± 0.00019	0.05750 ± 0.00306	7.3254 ± 0.0166
	2015 KJ64	13.9		5.29173 ± 0.00014	0.04005 ± 0.00003	7.4752 ± 0.0011
	2015 KW64	14.4		5.28895 ± 0.00080	0.04935 ± 0.00025	7.2849 ± 0.0038
	2016 GD174	14.5		5.29823 ± 0.00050	0.04635 ± 0.00008	7.3161 ± 0.0049
	2016 GP150	14.3		5.30621 ± 0.00063	0.05609 ± 0.00044	7.4113 ± 0.0044

continuation on next page

nr	prov. des.	H ^[1]	D [km] ^[2]	a_{prop} [au] ^[3]	e_{prop} ^[3]	i_{prop} [°] ^[3]
	2016 GZ187	14.4		5.29642 ± 0.00100	0.04528 ± 0.00019	7.3540 ± 0.0095
	2016 HQ11	14		5.31741 ± 0.00217	0.05620 ± 0.00056	7.4115 ± 0.0393
	2016 KN9	14.4		5.30576 ± 0.00037	0.04687 ± 0.00010	7.3294 ± 0.0024
	2015 FM155	14.2		5.28549 ± 0.00046	0.03636 ± 0.00011	7.2391 ± 0.0011

Table 4: Color data for Eurybates family members identified by the hierarchical clustering method (HCM) including the likely interloper (5258). The table gives the asteroid number (#), the provisional designation (prov. des.), the absolute magnitude (H), the diameter (D), as well as the g-i color from the Sloan Digital Sky Survey, the spectral slopes between 0.3 to 0.9 μ m (S), and the g-r color from the Zwicky Transient Facility Observations, ZTF. A machine readable version of this table is available on <https://zenodo.org/SOME-LINK>

- [1] Minor Planet Center; 2020-12-08, <https://minorplanetcenter.net//iau/lists/JupiterTrojans.html>
 [2] NEOWISE data v2.0, [Mainzer et al. \(2019\)](https://sbn.psi.edu/pds/resource/neowisediam.html), <https://sbn.psi.edu/pds/resource/neowisediam.html>
 [4] Sloan Digital Sky Survey (SDSS) Moving Object Catalog ([Ivezić et al., 2001](https://sbn.psi.edu/pds/resource/sdssmoc.html)), <https://sbn.psi.edu/pds/resource/sdssmoc.html>
 [5] [Fornasier et al. \(2007\)](https://sbn.psi.edu/pds/resource/fornasier.html), <https://sbn.psi.edu/pds/resource/fornasier.html>
 [6] [Schemel & Brown \(2021\)](https://sbn.psi.edu/pds/resource/fornasier.html)

nr	prov. des.	H ^[1]	D [km] ^[2]	g-i [mag] ^[4]	S [%/10 ³ Å] ^[5]	g-r [mag] ^[6]
3548	1973 SO	9.85	63.885 ± 0.299		-0.18 ± 0.57	0.51 ^{+0.02} _{-0.02}
5258	1989 AU1	10.33	53.275 ± 4.429			0.6 ^{+0.02} _{-0.02}
8060	1973 SD1	10.95	37.873 ± 0.567			0.51 ^{+0.02} _{-0.02}
9818	6591 P-L	11.07	28.076 ± 3.215	0.64 ± 0.022	2.12 ± 0.72	0.49 ^{+0.03} _{-0.04}
13862	1999 XT160	11.6	24.835 ± 0.589		1.59 ± 0.7	0.46 ^{+0.05} _{-0.04}
18060	1999 XJ156	11.12	36.431 ± 3.966	0.69 ± 0.045	2.86 ± 0.6	0.51 ^{+0.04} _{-0.05}
24380	2000 AA160	11.2	31.607 ± 0.266		0.34 ± 0.65	0.51 ^{+0.02} _{-0.02}
24420	2000 BU22	11.45	21.723 ± 1.211		1.65 ± 0.7	0.55 ^{+0.04} _{-0.04}
24426	2000 CR12	12.13	14.336 ± 1.007	0.71 ± 0.054	4.64 ± 0.8	0.49 ^{+0.07} _{-0.07}
28958	2001 CQ42	12.18	21.577 ± 0.652		-0.04 ± 0.8	0.41 ^{+0.07} _{-0.07}
39285	2001 BP75	12.49	17.602 ± 0.499		0.25 ± 0.69	0.48 ^{+0.15} _{-0.13}
39795	1997 SF28	12.42	18.342 ± 0.742			0.54 ^{+0.11} _{-0.09}
43212	2000 AL113	12.2	19.212 ± 1.09	0.56 ± 0.028	1.19 ± 0.78	0.53 ^{+0.1} _{-0.09}
43436	2000 YD42	12.12				0.45 ^{+0.08} _{-0.08}
53469	2000 AX8	12.39	18.453 ± 0.354		0.17 ± 0.8	0.44 ^{+0.07} _{-0.06}
65150	2002 CA126	12.47			4.14 ± 0.7	
65225	2002 EK44	12.36	16.654 ± 0.234	0.64 ± 0.036	0.97 ± 0.85	0.46 ^{+0.1} _{-0.09}
88229	2001 BZ54	12.32				0.39 ^{+0.07} _{-0.07}
111805	2002 CZ256	12.58		0.605 ± 0.025		0.48 ^{+0.14} _{-0.12}
127846	2003 FO111	12.47				0.54 ^{+0.1} _{-0.1}
160856	2001 DU92	12.59	16.216 ± 0.54			0.5 ^{+0.07} _{-0.07}
163135	2002 CT22	12.58	16.661 ± 0.735		2.76 ± 0.73	
163189	2002 EU6	12.9	16.23 ± 0.781			0.53 ^{+0.17} _{-0.14}
163216	2002 EN68	12.55	13.25 ± 0.801		3.6 ± 0.98	0.52 ^{+0.1} _{-0.09}
166211	2002 EP135	12.88	14.412 ± 1.052			0.57 ^{+0.15} _{-0.14}
191088	2002 CP286	12.95		0.8 ± 0.072		0.5 ^{+0.16} _{-0.14}
192388	1996 RD29	12.91			2.76 ± 0.89	
192929	2000 AT44	12.5	13.339 ± 0.482		-0.53 ± 0.83	
195412	2002 GF39	12.45	19.051 ± 0.439			0.46 ^{+0.08} _{-0.07}
200024	2007 OO7	12.8	13.808 ± 0.886			0.55 ^{+0.16} _{-0.14}
200032	2007 PU43	12.89	17.945 ± 0.582			0.6 ^{+0.15} _{-0.15}
210237	2007 RQ154	12.75	16.698 ± 0.713			0.5 ^{+0.11} _{-0.09}
214376	2005 LF20	13.06				0.52 ^{+0.17} _{-0.15}
219835	2002 CH82	13.29		0.72 ± 0.05		
223251	2003 FB70	12.6	17.702 ± 0.529	0.63 ± 0.042		
237035	2008 SL91	13.37	11.96 ± 0.773			0.59 ^{+0.16} _{-0.14}
246145	2007 PE9	13.21	12.093 ± 0.601			0.46 ^{+0.14} _{-0.12}
252683	2002 AE166	13		0.58 ± 0.028		
252711	2002 CU152	13.2		0.59 ± 0.057		
259316	2003 FJ38	13.9		0.53 ± 0.078		
313024	2000 AV210	13.6	10.805 ± 0.599	0.96 ± 0.092		

Acknowledgments

The work in this paper was supported by the Lucy mission through NASA's Discovery Program grant NNM16AA08C.

R.M. and H.F.L. acknowledge the support from NASA's Emerging Worlds program, grant NNX17AE83G.

R.M. also acknowledges the support from the Swiss National Science Foundation (SNSF) under the grant P2BEP2_184482.

D.N. acknowledges support from NASA SSW.

The work of R.D. was supported by the NASA's Emerging Worlds program, grant 80NSSC21K0387.

I.W. is supported by an appointment to the NASA Postdoctoral Program at the NASA Goddard Space Flight Center, administered by Oak Ridge Associated Universities under contract with NASA.

References

- Benavidez, P. G., Campo Bagatin, A., Curry, J., Álvarez-Candal, Á., & Vincent, J.-B. 2022, MNRAS, 514, 4876, doi: [10.1093/mnras/stac1578](https://doi.org/10.1093/mnras/stac1578)
- Benavidez, P. G., Durda, D. D., Enke, B., et al. 2018, Icarus, 304, 143, doi: [10.1016/j.icarus.2017.05.030](https://doi.org/10.1016/j.icarus.2017.05.030)
- Benavidez, P. G., Durda, D. D., Enke, B. L., et al. 2012, Icarus, 219, 57, doi: [10.1016/j.icarus.2012.01.015](https://doi.org/10.1016/j.icarus.2012.01.015)
- Benz, W., & Asphaug, E. 1999, Icarus, 142, 5, doi: [10.1006/icar.1999.6204](https://doi.org/10.1006/icar.1999.6204)
- Bottke, W. F., Brož, M., O'Brien, D. P., et al. 2015, The Collisional Evolution of the Main Asteroid Belt, 701–724, doi: [10.2458/azu_uapress_9780816532131-ch036](https://doi.org/10.2458/azu_uapress_9780816532131-ch036)
- Bottke, W. F., Durda, D. D., Nesvorný, D., et al. 2005, Icarus, 175, 111, doi: [10.1016/j.icarus.2004.10.026](https://doi.org/10.1016/j.icarus.2004.10.026)
- Bottke, W. F., Vokrouhlický, D., Ballouz, R. L., et al. 2020, AJ, 160, 14, doi: [10.3847/1538-3881/ab88d3](https://doi.org/10.3847/1538-3881/ab88d3)
- Brož, M., & Rozehnal, J. 2011, MNRAS, 414, 565, doi: [10.1111/j.1365-2966.2011.18420.x](https://doi.org/10.1111/j.1365-2966.2011.18420.x)
- Brown, M. E., Levison, H. F., Noll, K. S., et al. 2021, arXiv e-prints, arXiv:2106.02079. <https://arxiv.org/abs/2106.02079>
- Buie, M. W., Zangari, A. M., Marchi, S., Levison, H. F., & Mottola, S. 2018, 155, 245, doi: [10.3847/1538-3881/aabd81](https://doi.org/10.3847/1538-3881/aabd81)
- Davis, D. R., Durda, D. D., Marzari, F., Campo Bagatin, A., & Gil-Hutton, R. 2002, Collisional Evolution of Small-Body Populations, 545–558
- Di Sisto, R. P., Ramos, X. S., & Beaugé, C. 2014, Icarus, 243, 287, doi: [10.1016/j.icarus.2014.09.002](https://doi.org/10.1016/j.icarus.2014.09.002)
- Dohnanyi, J. S. 1969, J. Geophys. Res., 74, 2531, doi: [10.1029/JB074i010p02531](https://doi.org/10.1029/JB074i010p02531)
- Durda, D. D., Bottke, W. F., Enke, B. L., et al. 2004, Icarus, 170, 243, doi: [10.1016/j.icarus.2004.04.003](https://doi.org/10.1016/j.icarus.2004.04.003)
- Durda, D. D., Bottke, W. F., Nesvorný, D., et al. 2007, Icarus, 186, 498, doi: [10.1016/j.icarus.2006.09.013](https://doi.org/10.1016/j.icarus.2006.09.013)
- Emery, J. P., Burr, D. M., & Cruikshank, D. P. 2011, AJ, 141, 25, doi: [10.1088/0004-6256/141/1/25](https://doi.org/10.1088/0004-6256/141/1/25)
- Emery, J. P., Marzari, F., Morbidelli, A., French, L. M., & Grav, T. 2015, The Complex History of Trojan Asteroids, 203–220, doi: [10.2458/azu_uapress_9780816532131-ch011](https://doi.org/10.2458/azu_uapress_9780816532131-ch011)
- Fornasier, S., Dotto, E., Hainaut, O., et al. 2007, Icarus, 190, 622, doi: [10.1016/j.icarus.2007.03.033](https://doi.org/10.1016/j.icarus.2007.03.033)

- Fornasier, S., Hasselmann, P. H., Barucci, M. A., et al. 2015, *A&A*, 583, A30, doi: [10.1051/0004-6361/201525901](https://doi.org/10.1051/0004-6361/201525901)
- Gomes, R., Levison, H. F., Tsiganis, K., & Morbidelli, A. 2005, *Nature*, 435, 466, doi: [10.1038/nature03676](https://doi.org/10.1038/nature03676)
- Grav, T., Mainzer, A. K., Bauer, J., et al. 2011, *ApJ*, 742, 40, doi: [10.1088/0004-637X/742/1/40](https://doi.org/10.1088/0004-637X/742/1/40)
- Holsapple, K., & Housen, K. 1986, *Memorie della Societa Astronomica Italiana*, 57, 65
- Holsapple, K. A., & Housen, K. R. 2019, *Planet. Space Sci.*, 179, 104724, doi: [10.1016/j.pss.2019.104724](https://doi.org/10.1016/j.pss.2019.104724)
- Holt, T. R., Nesvorný, D., Horner, J., et al. 2020, *MNRAS*, 495, 4085, doi: [10.1093/mnras/staa1348](https://doi.org/10.1093/mnras/staa1348)
- Ivezić, Ž., Tabachnik, S., Rafikov, R., et al. 2001, *AJ*, 122, 2749, doi: [10.1086/323452](https://doi.org/10.1086/323452)
- Jewitt, D. 2018, *AJ*, 155, 56, doi: [10.3847/1538-3881/aaa1a4](https://doi.org/10.3847/1538-3881/aaa1a4)
- Jewitt, D. C., Trujillo, C. A., & Luu, J. X. 2000, *AJ*, 120, 1140, doi: [10.1086/301453](https://doi.org/10.1086/301453)
- Jutzi, M. 2015, *Planetary and Space Science*, 107, 3, doi: [10.1016/j.pss.2014.09.012](https://doi.org/10.1016/j.pss.2014.09.012)
- Jutzi, M., Michel, P., Benz, W., & Richardson, D. C. 2010, *Icarus*, 207, 54, doi: [10.1016/j.icarus.2009.11.016](https://doi.org/10.1016/j.icarus.2009.11.016)
- Jutzi, M., Michel, P., & Richardson, D. C. 2019, *Icarus*, 317, 215, doi: [10.1016/j.icarus.2018.08.006](https://doi.org/10.1016/j.icarus.2018.08.006)
- Klahr, H., & Schreiber, A. 2020, *ApJ*, 901, 54, doi: [10.3847/1538-4357/abac58](https://doi.org/10.3847/1538-4357/abac58)
- . 2021, *ApJ*, 911, 9, doi: [10.3847/1538-4357/abca9b](https://doi.org/10.3847/1538-4357/abca9b)
- Lagrange, J.-L. 1772, *Prix de l'académie royale des Sciences de paris*, 9, 292
- Leinhardt, Z. M., & Stewart, S. T. 2009, *Icarus*, 199, 542, doi: [10.1016/j.icarus.2008.09.013](https://doi.org/10.1016/j.icarus.2008.09.013)
- Levison, H. F., Olkin, C., Noll, K. S., Marchi, S., & Lucy Team. 2017, in *Lunar and Planetary Science Conference, Lunar and Planetary Science Conference, 2025*
- Levison, H. F., Shoemaker, E. M., & Shoemaker, C. S. 1997, *Nature*, 385, 42, doi: [10.1038/385042a0](https://doi.org/10.1038/385042a0)
- Mainzer, A. K., Bauer, J. M., Cutri, R. M., et al. 2019, *NASA Planetary Data System*, doi: [10.26033/18S3-2Z54](https://doi.org/10.26033/18S3-2Z54)
- Marzari, F., Scholl, H., Murray, C., & Lagerkvist, C. 2002, *Origin and Evolution of Trojan Asteroids*, 725–738
- Michel, P., Benz, W., Tanga, P., & Richardson, D. C. 2001, *Science*, 294, 1696
- Milani, A., Knežević, Z., Spoto, F., et al. 2017, *Icarus*, 288, 240, doi: [10.1016/j.icarus.2016.12.030](https://doi.org/10.1016/j.icarus.2016.12.030)
- Morbidelli, A., Bottke, W. F., Nesvorný, D., & Levison, H. F. 2009a, *Icarus*, 204, 558, doi: [10.1016/j.icarus.2009.07.011](https://doi.org/10.1016/j.icarus.2009.07.011)
- Morbidelli, A., Levison, H. F., Bottke, W. F., Dones, L., & Nesvorný, D. 2009b, *Icarus*, 202, 310, doi: [10.1016/j.icarus.2009.02.033](https://doi.org/10.1016/j.icarus.2009.02.033)
- Morbidelli, A., Levison, H. F., Tsiganis, K., & Gomes, R. 2005, *Nature*, 435, 462, doi: [10.1038/nature03540](https://doi.org/10.1038/nature03540)
- Morbidelli, A., Nesvorný, D., Bottke, W. F., & Marchi, S. 2021, *Icarus*, 356, 114256, doi: [10.1016/j.icarus.2020.114256](https://doi.org/10.1016/j.icarus.2020.114256)
- Mottola, S., Hellmich, S., Buie, M. W., et al. 2020, *The Planetary Science Journal*, 1, 73, doi: [10.3847/PSJ/abb942](https://doi.org/10.3847/PSJ/abb942)

- Nesvorný, D., Brož, M., & Carruba, V. 2015, Identification and Dynamical Properties of Asteroid Families, 297–321, doi: [10.2458/azu_uapress_9780816532131-ch016](https://doi.org/10.2458/azu_uapress_9780816532131-ch016)
- Nesvorný, D., Enke, B. L., Bottke, W. F., et al. 2006, *Icarus*, 183, 296, doi: [10.1016/j.icarus.2006.03.008](https://doi.org/10.1016/j.icarus.2006.03.008)
- Nesvorný, D., Vokrouhlický, D., Bottke, W. F., & Levison, H. F. 2018, *Nature Astronomy*, 2, 878, doi: [10.1038/s41550-018-0564-3](https://doi.org/10.1038/s41550-018-0564-3)
- Nesvorný, D., Vokrouhlický, D., Bottke, W. F., Noll, K., & Levison, H. F. 2011, *AJ*, 141, 159, doi: [10.1088/0004-6256/141/5/159](https://doi.org/10.1088/0004-6256/141/5/159)
- Nesvorný, D., Vokrouhlický, D., & Morbidelli, A. 2013, *ApJ*, 768, 45, doi: [10.1088/0004-637X/768/1/45](https://doi.org/10.1088/0004-637X/768/1/45)
- Noll, K. S., Brown, M. E., Weaver, H. A., et al. 2020, *The Planetary Science Journal*, 1, 44, doi: [10.3847/PSJ/abac54](https://doi.org/10.3847/PSJ/abac54)
- O'Brien, D. P., & Greenberg, R. 2003, *Icarus*, 164, 334, doi: [10.1016/S0019-1035\(03\)00145-3](https://doi.org/10.1016/S0019-1035(03)00145-3)
- Pirani, S., Johansen, A., & Mustill, A. J. 2019, *A&A*, 631, A89, doi: [10.1051/0004-6361/201936600](https://doi.org/10.1051/0004-6361/201936600)
- Robutel, P., & Gabern, F. 2006, *MNRAS*, 372, 1463, doi: [10.1111/j.1365-2966.2006.11008.x](https://doi.org/10.1111/j.1365-2966.2006.11008.x)
- Roig, F., Ribeiro, A. O., & Gil-Hutton, R. 2008, *A&A*, 483, 911, doi: [10.1051/0004-6361:20079177](https://doi.org/10.1051/0004-6361:20079177)
- Rozehnal, J., Brož, M., Nesvorný, D., et al. 2016, *MNRAS*, 462, 2319, doi: [10.1093/mnras/stw1719](https://doi.org/10.1093/mnras/stw1719)
- Schemel, M., & Brown, M. E. 2021, *Planetary Science Journal*, 2, 40, doi: [10.3847/PSJ/abc752](https://doi.org/10.3847/PSJ/abc752)
- Senft, L. E., & Stewart, S. T. 2007, *Journal of Geophysical Research (Planets)*, 112, E11002, doi: [10.1029/2007JE002894](https://doi.org/10.1029/2007JE002894)
- . 2008, *Meteoritics and Planetary Science*, 43, 1993, doi: [10.1111/j.1945-5100.2008.tb00657.x](https://doi.org/10.1111/j.1945-5100.2008.tb00657.x)
- Singer, K. N., McKinnon, W. B., Gladman, B., et al. 2019, *Science*, 363, 955, doi: [10.1126/science.aap8628](https://doi.org/10.1126/science.aap8628)
- Szabó, G. M., Ivezić, Ž., Jurić, M., & Lupton, R. 2007, *MNRAS*, 377, 1393, doi: [10.1111/j.1365-2966.2007.11687.x](https://doi.org/10.1111/j.1365-2966.2007.11687.x)
- Tsiganis, K., Gomes, R., Morbidelli, A., & Levison, H. F. 2005, *Nature*, 435, 459, doi: [10.1038/nature03539](https://doi.org/10.1038/nature03539)
- Wong, I., & Brown, M. E. 2015, *AJ*, 150, 174, doi: [10.1088/0004-6256/150/6/174](https://doi.org/10.1088/0004-6256/150/6/174)
- . 2016, *AJ*, 152, 90, doi: [10.3847/0004-6256/152/4/90](https://doi.org/10.3847/0004-6256/152/4/90)
- Wong, I., Brown, M. E., & Emery, J. P. 2014, *AJ*, 148, 112, doi: [10.1088/0004-6256/148/6/112](https://doi.org/10.1088/0004-6256/148/6/112)
- Yoshida, F., & Nakamura, T. 2008, *Publications of the Astronomical Society of Japan*, 60, 297, doi: [10.1093/pasj/60.2.297](https://doi.org/10.1093/pasj/60.2.297)
- Yoshida, F., & Terai, T. 2017, *The Astronomical Journal*, 154, 71, doi: [10.3847/1538-3881/aa7d03](https://doi.org/10.3847/1538-3881/aa7d03)
- Youdin, A. N., & Goodman, J. 2005, *ApJ*, 620, 459, doi: [10.1086/426895](https://doi.org/10.1086/426895)
- Zappala, V., Cellino, A., Farinella, P., & Knezevic, Z. 1990, *AJ*, 100, 2030, doi: [10.1086/115658](https://doi.org/10.1086/115658)